J. Wind Eng. Ind. Aerodyn. 151 (2016) 1–24

Contents lists available at ScienceDirect

Journal of Wind Engineering and Industrial Aerodynamics

journal homepage: www.elsevier.com/locate/jweia

Study of the effects of translation and roughness on tornado-like vortices by large-eddy simulations

Zhenqing Liu [a,*], Takeshi Ishihara [b]

[a] School of Civil Engineering and Mechanics, Huazhong University of Science and Technology, Wuhan, Hubei, China
[b] Department of Civil Engineering, School of Engineering, The University of Tokyo, Tokyo, Japan

ARTICLE INFO

Article history:
Received 6 July 2015
Received in revised form
2 January 2016
Accepted 2 January 2016

Keywords:
Tornado-like vortex
Turbulent flow fields
LES
Reynolds stresses
Translation
Roughness
Swirl ratio
Similarity

ABSTRACT

The numerical simulation by LES turbulent model for translating tornadoes and those over roughness was carried out in a Ward type simulator. The tornado translation was modeled by providing a relative motion on the ground and the roughness was simulated through adding a momentum source in the Navier–Stokes equation. The effects of translation and roughness on the flow fields of three typical tornado-like vortices, i.e., vortex breakdown, vortex touching down and multi-vortex, were investigated and the detailed velocity distributions, Reynolds stresses and the pressure on the ground were examined. The similarity of the flow fields after the introduction of translation and ground roughness was also studied. It was found that, at the high elevation, V_c and r_c shows the same trend versus the external swirl ratio for stationary and translating tornadoes. However, if the ground is rough, the core radius at high elevation changes greatly. The ground roughness will expand the size of the core. But for the very small swirl ratio cases, the ground roughness shows the effect reducing the core size. The explanation for the evolution of the flow fields due to translation and ground roughness is provided.

1. Introduction

Researchers have conducted intensive studies concerning flow structures, dynamics and similarity of tornado-like vortices. Consequently, a large number of significant findings have been obtained, such as dominant parameters determining flow structure (see, e.g., Ward (1972), Rotunno (1977), Church et al. (1979) and Kuai et al. (2008)), organized swirl motion in tornadoes (see, e.g., Monji (1985), and Ishihara and Liu (2014)) and similarity between simulated tornadoes and those in nature (see, e.g., Hangan and Kim (2008) and Liu and Ishihara (2015a)). The majority of these studies focus on the stationary tornadoes on smooth ground. However, tornadoes in nature are frequently observed with a translation speed ranging from 10 m/s to 30 m/s, such as the tornado took place in Spencer, South Dakota, the US in 1998, which was observed by Wurman and Alexander (2005). Furthermore, tornados can also occur in urban area, such as the tornado occurred in Joplin, Missouri, the US in 2011, which was reported by Doswell et al. (2012).

By adding a movable ground plate in Ward type simulator, translation effects were studied by Diamond and Wilkins (1984) experimentally and secondary vortices were found to be generated by the translation. Most recently, through large eddy simulation, the effect of tornado translation was investigated by Natarajan and Hangan (2012) in a larger range of swirl ratio. In addition, the method simulating tornado translation is same as that in the study performed by Diamond and Wilkins (1984) who found that the effect was not uniform across external swirl ratios. However, there was no quantitative explanation regarding translation effects on tornado configuration.

In order to study how surface roughness has an influence on velocities, pressure and core radius, a large number of researches have been performed. However, researchers are not in complete agreement on how the roughness affects them. As found by Diamond and Wilkins (1984) and Zhang and Sarkar (2008), the vortex diameter decreases with the introduction of ground roughness, while the results from Dessens (1972), Leslie (1977), Monji and Wang (1989) and Natarajan and Hangan (2012) demonstrate that the effect of increasing surface roughness was to enlarge the vortex core. Besides, the shrink mechanism or tornado size expansion due to roughness must be clarified.

By adopting LES model, flow fields of tornado-like vortices after the introduction of translation and roughness are investigated in this study, so as to shed light on the effects of these factors. In Section 2, the details of the model simulating tornado translation and roughness will be introduced, including dimension, grid distribution, boundary conditions and definitions of swirl ratio.

* Corresponding author.
E-mail addresses: liuzhenqing1984@hotmail.com (Z. Liu), ishihara@bridge.t.u-tokyo.ac.jp (T. Ishihara).

http://dx.doi.org/10.1016/j.jweia.2016.01.006
0167-6105/

Nomenclature

$a_{\tilde{u}}$	frontal area density of roughness
C_d	drag coefficient of roughness
h_R	height of roughness
$h_{v\ max}$	height at which V_{max} occurs
P_{min}	minimum pressure drop
r_0	radius of updraft hole of simulator
r_c	radius at which V_c occurs
$r_{v\ max}$	radius at which V_{max} occurs
S_c	local corner swirl ratio
S_E	external swirl ratio
U	mean radial velocity
U_{min}	minimum radial velocity
u'	r.m.s of fluctuating radial velocity
V	mean tangential velocity
V_c	maximum tangential velocity in the cyclostrophic balance region
V_{max}	maximum tangential velocity
v_T	translation speed of tornado
v'	r.m.s of fluctuating tangential velocity
W	mean vertical velocity
W_0	upward velocity at outlet of simulator
W_{max}	maximum vertical velocity
w'	r.m.s of fluctuating vertical velocity

Section 3 provides a general view of the effects from tornado translation and ground roughness. In Section 4 and Section 5, the translation and roughness effects on the flow fields of tornado-like vortices and their mechanisms will be discussed. The detailed information of the mean flow fields and the Reynolds Stresses will be also provided.

2. Numerical model

The governing equations will be introduced in Section 2.1. Section 2.2 will provide the detailed information of the configurations for the numerical tornado simulator. Boundary conditions and the solution schemes will be presented in Sections 2.3 and 2.4. The methods simulating tornado translation and surface roughness will be introduced in Sections 2.5 and 2.6. Section 2.7 gives the definitions of swirl ratio.

2.1. Governing equations

As momentum and mass are mainly transported by large eddies, large eddy simulation (LES) is employed to simulate the tornado-like vortex in consideration of the current computing capability. In LES, large eddies are computed directly, while the influence of eddies smaller than grid spacing are modeled. Although LES is computationally expensive, it can provide detailed and accurate information. In addition, standard Smagorinsky–Lilly model is adopted to calculate subgrid-scale (SGS) stresses.

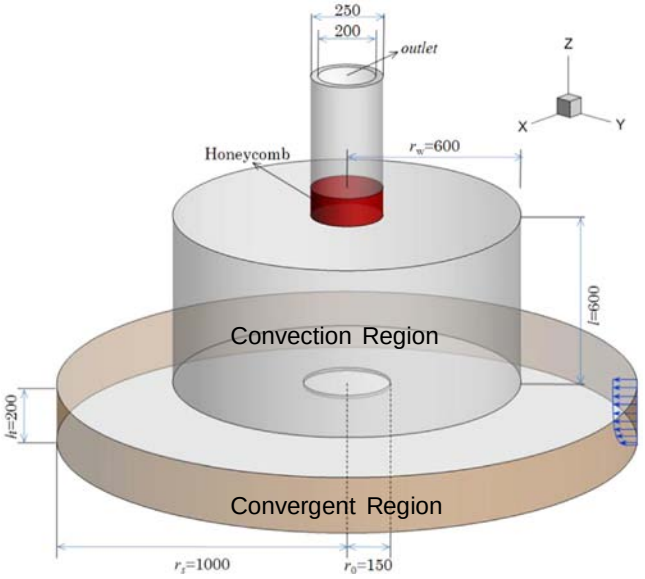

Fig. 1. Geometry of the model. Red color shows the location of honeycomb. Arrows indicate the direction of flow at the inlet. (For interpretation of the references to color in this figure legend, the reader is referred to the web version of this article.)

By filtering time-dependent Navier–Stokes equations in Cartesian coordinates (x, y, z), governing equations are obtained and expressed in the form of tensor as follows:

$$\frac{\partial \tilde{u}_i}{\partial x_i} = 0 \tag{1}$$

$$\rho\frac{\partial \tilde{u}_i}{\partial t} + \rho\frac{\partial \tilde{u}_i\tilde{u}_j}{\partial x_j} = \frac{\partial}{\partial x_j}\left(\mu\frac{\partial \tilde{u}_i}{\partial x_j}\right) - \frac{\partial \tilde{p}}{\partial x_i} - \frac{\partial \tau_{ij}}{\partial x_j} \tag{2}$$

of which $\tilde{u}_i$ and $\tilde{p}$ are respectively filtered velocities and pressure, μ is viscosity, ρ is density, τ_{ij} is SGS stress and modeled as follows:

$$\tau_{ij} = -2\mu_t\tilde{S}_{ij} + \frac{1}{3}\tau_{kk}\delta_{ij}; \quad \tilde{S}_{ij} = \frac{1}{2}\left(\frac{\partial \tilde{u}_i}{\partial x_j} + \frac{\partial \tilde{u}_j}{\partial x_i}\right) \tag{3}$$

where μ_t denotes SGS turbulent viscosity and $\tilde{S}_{ij}$ is the rate-of-strain tensor for the resolved scale, δ_{ij} is the Kronecker delta. Smagorinsky–Lilly model is employed for the SGS turbulent viscosity:

$$\mu_t = \rho L_s^2|\tilde{S}| = \rho L_s^2\sqrt{2\tilde{S}_{ij}\tilde{S}_{ij}}, \quad L_s = min\left(\kappa d, C_s V^{\frac{1}{3}}\right) \tag{4}$$

in which L_s denotes the mixing length for subgrid-scales, κ is the von Kármán constant, 0.42, d is the distance to the closest wall and V is the volume of a computational cell. C_s is Smagorinsky constant. In this study, C_s is determined as 0.032 based on the study performed by Ishihara and Liu (2014) and (2015a). In those studies, the flow fields of tornado like vortices in simulation have shown good agreements with experiments. The numerical simulators in the present study, the study by Ishihara and Liu (2014), (2015a), and (2015b) are same. Therefore, we would like to follow the previous studies and use the same C_s value. Following comparison with the observation data shows good agreement, see Fig. 19, which also verify C_s value used in the present study.

Table 1
Physical parameters of numerical tornado simulator.

Height of the inlet layer (h)	200 mm
Radius of the updraft hole (r_0)	150 mm
Internal aspect ratio ($a = h/r_0$)	1.33
Radius of the exhaust outlet (r_t)	100 mm
Radius of the convergence region (r_s)	1000 mm
Velocity at the outlet (W_0)	9.55 m/s$^-$
Total outflow rate ($Q = \pi r_t^2 W_0$)	0.3 m^3/s
Reynolds number ($Re = 2r_0W_0/\nu$)	1.60×10^5

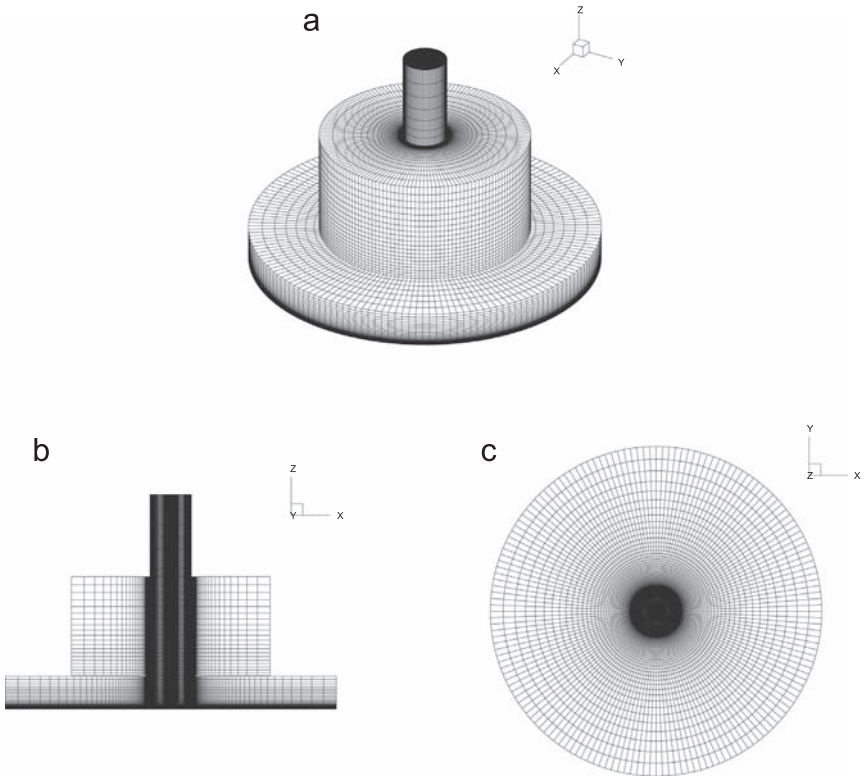

Fig. 2. Mesh of the numerical model: (a) isometric view, (b) lateral view, and (c) bird's-eye view.

Table 2
Mesh parameters of numerical tornado simulator.

Mesh size in the radial direction	1.0–25.0 mm
Mesh size in the vertical direction	0.1–5.0 mm
Mesh number for translation cases	784,200
Mesh number for roughness cases	1,023,600
Maximum y+ on the bottom of simulator	2.0

Table 3
Boundary conditions of numerical tornado simulator.

Simulator walls	Wall function, $u=0$,$v=0$,$w=0$, $\partial p/\partial n=0$
Inlet of simulator	u, v, w are determined by wind profiles in Eq. (7), $p=0$
Outlet of simulator	$\partial p/\partial n=0$, $\partial u/\partial n=0$, $\partial v/\partial n=0$, $\partial w/\partial n=0$
Honeycomb	Porous media is applied; drag force coefficient in z direction is 0; drag force coefficients in horizontal directions are 2000.

2.2. Configurations and mesh of the numerical tornado simulator

In this study, the Ward-type simulator used in the experimental study performed by Matsui and Tamura (2009) is chosen and guide vanes are removed, see Fig. 1. As shown in Eq. (7), the wind profile at inlet is used to vary the swirl strength. Two significant geometry parameters are the height of the inlet, h, and the radius of the updraft hole, r_0, which are respectively 200 mm and 150 mm. The flow rate is calculated as $Q=\pi r_t^2 W_0$, in which r_t is the radius of the exhaust outlet and W_0 is the velocity at the outlet. Following the tradition in the field of tornado researches and making it convenient to compare with previous studies, the Reynolds number is expressed as $Re=2r_0W_0/\nu$ in the present research. In Table 1, physical parameters used in this study are summarized.

In the vicinity of the center and the region near the ground, a fine mesh is considered in the domain of the convergent region, so as to investigate turbulent features quantitatively as shown in Fig. 2. In the center of the simulator, an unstructured mesh is adopted, which has been used in the study of Ishihara and Liu (2014) as well. Out of the circle with a diameter of 0.005 m, 80 nodes are used for translation cases and roughness cases in the radial direction. In vertical direction, 45 nodes for translation cases and 60 nodes for roughness cases are adopted. Moreover, the minimum size of the mesh is respectively about 1 mm and 0.1 mm in the radial and vertical direction. In order to avoid a sudden change of the grid size, spacing ratios are less than 1.2 in the two directions. Near the center of simulator, $0r_0 \le r \le 0.5r_0$, $0r_0 \le z \le 1r_0$, the radial spacing ration is 1.0 and vertical spacing ratio is only 1.05, because this region is the concern of our research and the flow there is most turbulent. However, the flow in the convection region is in the downstream of the modeled tornado-like vortices, therefore we applied coarse grids to discretize in space. The total mesh number is about 7.8×10^5 for translation cases and 1.0×10^6 for roughness cases. The treatment of the mesh at the top of the convergent zone and the boundary around the convection zone, i.e. coarse meshes there, is consistent with the study by Kim and Hangan (2007), Maruyama (2011), Ishihara et al. (2011), Ishihara and Liu (2014), and (2015a). These studies have shown good agreement with experiments, indicating that coarse meshes in the convection region do not have large influence to the core of tornado. We have compared the simulated flow field of the tornado like vortices over smooth ground with those by Ishihara and Liu (2014) in which the grid is coarser than the present study. The numerical results in the two simulations have shown good agreements with experiment by Matsui and Tamura (2009), indicating that the results are grid independent. The mesh parameters are listed in Table 2.

2.3. Boundary conditions

For the surfaces of the convergent zone, surfaces around the convection zone and the bottom of the simulator, consistent with

the previous study conducted by Liu and Ishihara (2015a), wall function is applied. When wall-adjacent cells are in the laminar sublayer, wall shear stresses are obtained from the laminar stress–strain relationship:

$$\frac{\tilde{u}}{u_\tau}=\frac{\rho u_\tau y}{\mu} \tag{5}$$

Provided that the mesh cannot resolve the laminar sublayer, the centroid of the wall-adjacent cells is assumed to fall within the logarithmic region of the boundary layer, and the law-of-the-wall is employed as follows:

$$\frac{\tilde{u}}{u_\tau}=\frac{1}{\kappa}\ln E\left(\frac{\rho u_\tau d}{\mu}\right) \tag{6}$$

where $\tilde{u}$ is the filtered velocity tangential to wall, d is the distance between the center of the cell and the wall, u_τ is the friction velocity, and the constant E is 9.793. In tornado-like vortices, a flow with both axial and radial pressure gradients is present; however, the radial pressure gradient dominates the axial pressure gradient in the near-surface region, which implies the wall function can be used. In most of the region, the wall-adjacent cells are in the laminar sublayer. The maximum y+ on the bottom of tornado simulator is 2.

For the inlet, velocity profiles are specified as below:

$$\begin{cases} u_{rs}=u_1\dfrac{z}{z_1}^{1/n} \\ v_{rs}=-u_{rs}\ \tan(\theta) \end{cases} \tag{7}$$

where u_{rs} and v_{rs} are radial velocities and tangential velocities at $r=r_s$ (see Fig. 1), n is equal to 7, reference velocity U_1 and reference height z_1 are respectively set to 0.24 m/s and 0.01 m, by matching the velocity profile at the inner ring of the guide vanes in Ishihara et al. (2011), and θ is the inflow angle. In Eq. (7), U_1 is a constant. Moreover, u_{rs} is a function of z. The inflow angle θ is adjusted to change the swirl ratio.

For the honeycomb, porous media is applied to model, in which no drag force is added in the vertical momentum equation but almost infinite drag forces are added in the horizontal directions. The drag force coefficients of the honeycomb in the horizontal directions are set as 2000. Therefore, the fluid can move freely in vertical direction with nearly no motion in the horizontal directions, which is similar to fluid in a honeycomb.

For the outlet, the outflow boundary condition is used, which means that normal gradients in pressure and velocities are set to zero here (Table 3).

2.4. Solution scheme

A finite volume method is employed for the present simulations. Furthermore, the second order central difference scheme is used for the convective and viscosity term, while the second order implicit scheme is used for the unsteady term. Semi-implicit pressure linked equations (SIMPLE) algorithm is employed to solve the discretized equations (Ferziger and Peric, 2002). The courant number (CFL) is 1.0. Table 4 summarizes the solution parameters in this study.

After 10 s, initial transient effects were found to disappear. Therefore, the data for time sampling begin at 10 s and then flow

Table 4
Solution parameters of numerical tornado simulator.

Turbulence model	LES Smagorinsky–Lilly (Cs=0.032)
Spatial discretization method	Finite volume method Second order central difference scheme
Time discretization scheme	Second order implicit scheme
Decoupling algorithm	SIMPLE
CFL number	1.0

Table 5
Parameters for modeling tornado translation.

Translation speed added at the bottom of simulator (v_T)	3.3 m/s
Translation speed in full scale (V_T)	10 m/s
Velocity scale	1:3.05

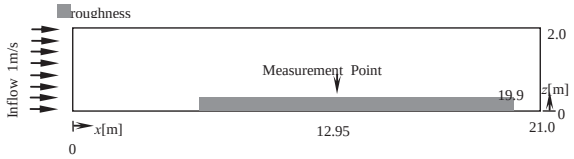

Fig. 4. Layout of the experiment for the boundary layer flow with ground roughness.

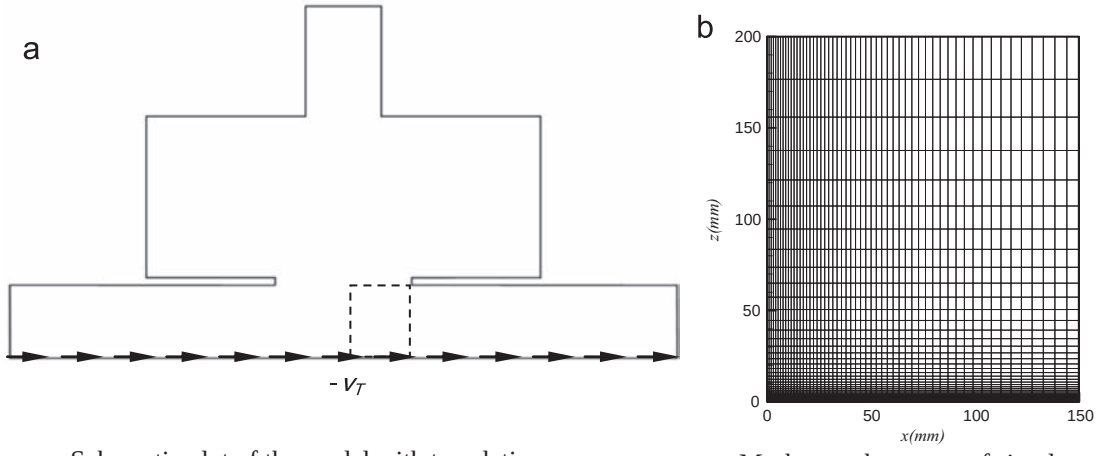

Schematic plot of the model with translation

Mesh near the center of simulator

Fig. 3. Schematic plot and the mesh of the model with translation. The arrows indicate the added velocity on the ground. v_T is the translation speed of tornado. "−" means the added velocity on the ground is opposite with the translation of the tornado. The velocity on the bottom is 3.3 m/s. The mesh in the region indicated by the dashed line is shown on the right hand side.

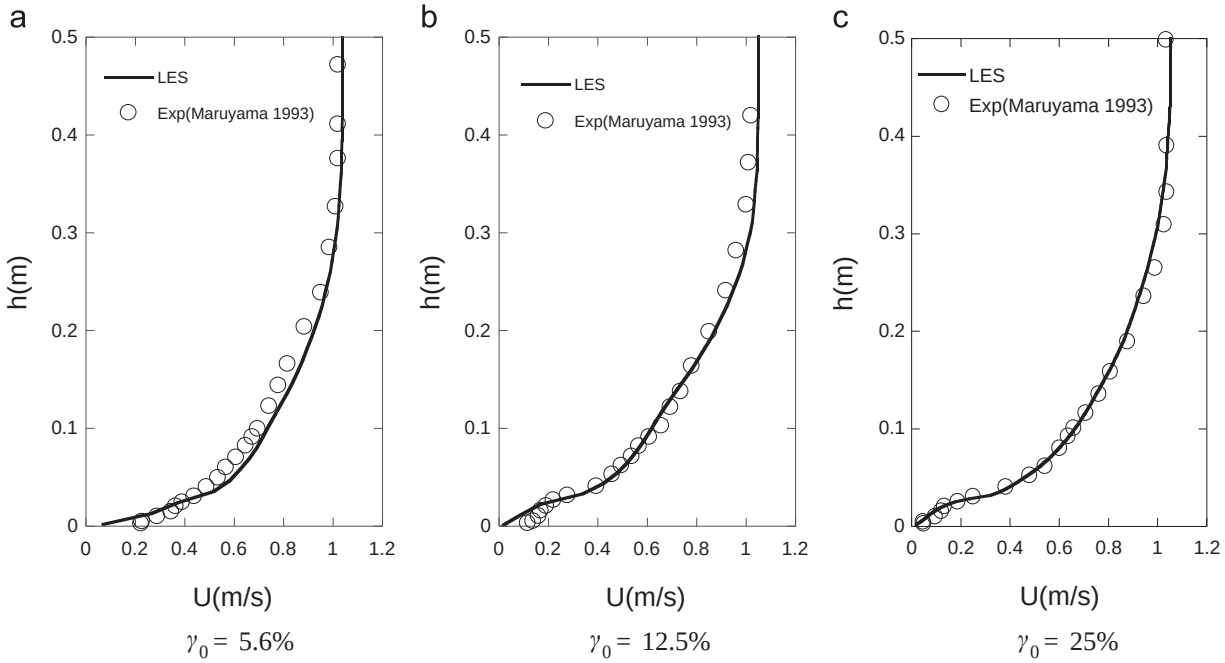

Fig. 5. Comparison of the profiles of mean wind speed over the roughness blocks at x=12.95 m with density of (a) 5.6%, (b) 12.5% and (c) 25%.

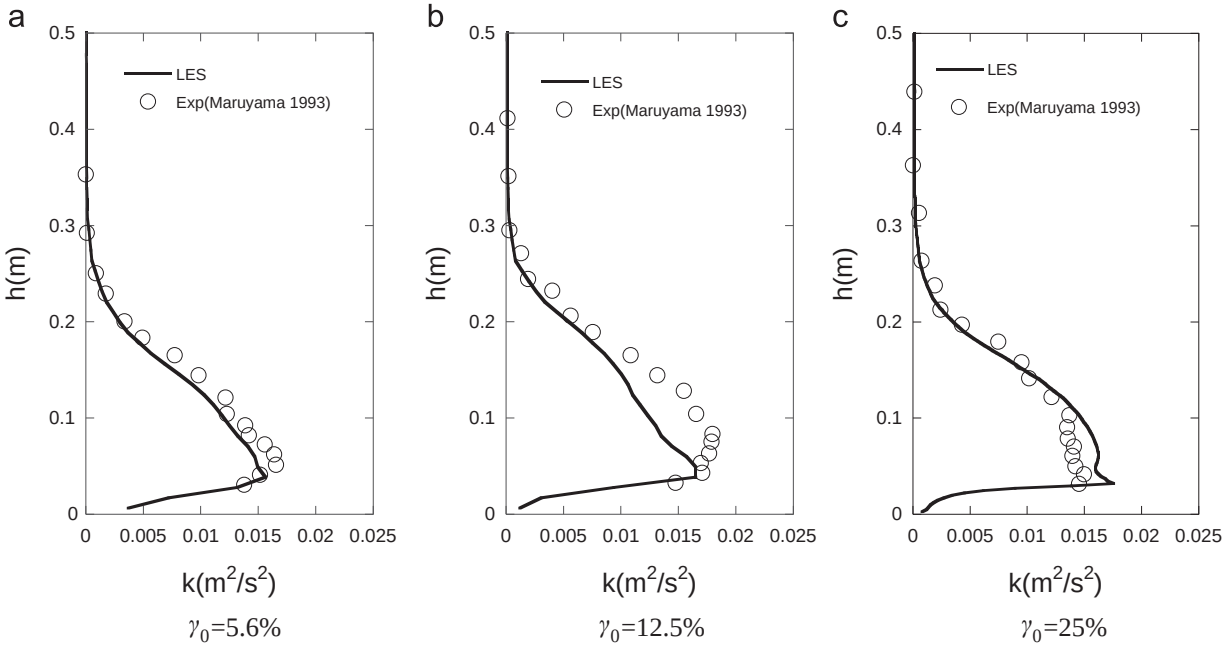

Fig. 6. Comparison of the profiles of kinetic energy over the roughness blocks at x=12.95 m with density of (a) 5.6%, (b) 12.5% and (c) 25%.

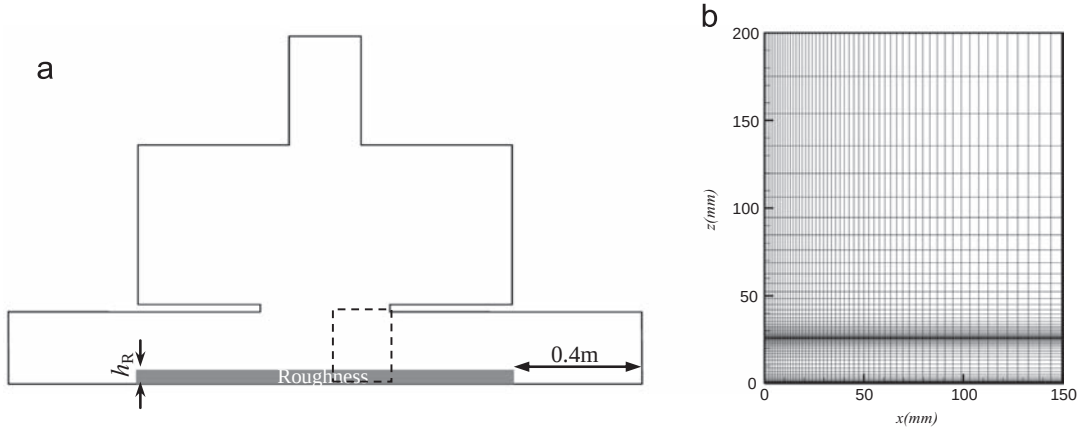

Fig. 7. Schematic plot and the mesh of the model with ground roughness. The gray filled region indicates the roughness, the height of this region is 0.026 m. The mesh in the region indicated by the dashed line is shown on the right hand side.

Table 6
Parameters for modeling tornado over rough ground.

Height of roughness added on the bottom (h_R)	0.026 m
Height of roughness in full scale, (H_R)	50 m
Length scale	1:1905
Volume density of roughness (γ_0)	0.056
Drag force coefficients ($C_{D,\hat{u}i}$)	$C_{D,\hat{u}x}=2.0$, $C_{D,\hat{u}y}=2.0$, $C_{D,\hat{u}z}=0.0$

Table 7
Case settings of the numerical simulations.

	Case name	θ (deg)	S_E	S_c
Stationary tornado over smooth ground	Case1	46.8	0.4	0.71
	Case2	58.0	0.6	1.59
	Case3	64.9	0.8	2.36
	Case4	69.4	1.0	2.93
	Case5	76.0	1.5	4.16
	Case6	79.4	2.0	5.39
	Case7	82.1	2.7	6.74
	Case8	83.5	3.3	7.96
	Case9	84.4	3.8	8.89
Translating tornado	$Case1_{,t}$	46.8	0.4	0.49
	$Case2_{,t}$	58.0	0.6	0.86
	$Case3_{,t}$	64.9	0.8	2.32
	$Case4_{,t}$	69.4	1.0	2.65
	$Case5_{,t}$	76.0	1.5	4.12
	$Case6_{,t}$	79.4	2.0	5.02
	$Case7_{,t}$	82.1	2.7	6.55
	$Case8_{,t}$	83.5	3.3	7.41
	$Case9_{,t}$	84.4	3.8	9.12
Tornado over rough ground	$Case1_{,r}$	46.8	0.4	0.24
	$Case2_{,r}$	58.0	0.6	0.56
	$Case3_{,r}$	64.9	0.8	1.67
	$Case4_{,r}$	69.4	1.0	2.14
	$Case5_{,r}$	76.0	1.5	3.51
	$Case6_{,r}$	79.4	2.0	4.92
	$Case7_{,r}$	82.1	2.7	6.13
	$Case8_{,r}$	83.5	3.3	6.77
	$Case9_{,r}$	84.4	3.8	8.10

*Simple "–" means the data is not available in the simulation. Subscripts "$_{,t}$" and "$_{,r}$" are used to distinguish the translating tornadoes and the tornadoes over rough ground, respectively.

fields are temporally averaged from 10 s to 30 s. By evaluating relative errors in the maximum mean tangential velocity within the cyclostrophic balance region, a stationary condition for time sampling can be achieved. When the data from 10 s to 30 s are used, V_c becomes less than 1%. Besides, the time sampling error is calculated by means of finding the difference of the time averaged result of V_c from 10 s to 10 s+T/2 and that from 10 s+T/2 to 10 s+T, in which T is the time used for time sampling. The cyclostrophic balance region is the height at which the centrifugal force balances the pressure gradient force. In this study, this region is located at a height of $z=r_0$.

2.5. Modeling translation

Since the apparatus is mounted on the ground and it is difficult to move the simulator, tornado translation is difficult to be simulated by Ward type simulator experimentally. A movable ground plate had been installed in the Ward type simulator by Diamond and Wilkins (1984), which could be propelled across the floor. In the large eddy simulation by Natarajan and Hangan (2012), they kept the vortex stationary and moved the base surface in a direction opposite to the vortex translation direction, thereby generating equivalent relative motion, which was consistent with the experiment implemented by Diamond and Wilkins (1984). In the present study, the method simulating tornado translation in previous studies is followed. While this relative motion argument is valid for the surface region of the flow, which is the region of interest, in real situation translation of a vortex refers to the movement of the vortex relative to the fixed surface. However, it can be said from the following validation (see Fig. 19) that the method simulating tornado translation in the present study is applicable to consider the effects on flow fields near the surface. In this study, a translation speed of $v_T=3.3$ m/s is introduced on the ground surface, see Fig. 3(a), which corresponds to the speed of $V_T=10$ m/s in full scale. As the velocity scale of this numerical tornado simulator is identified as 1:3.05 as to be presented in the following discussion. Parameters modeling the translation of tornado are listed in Table 5.

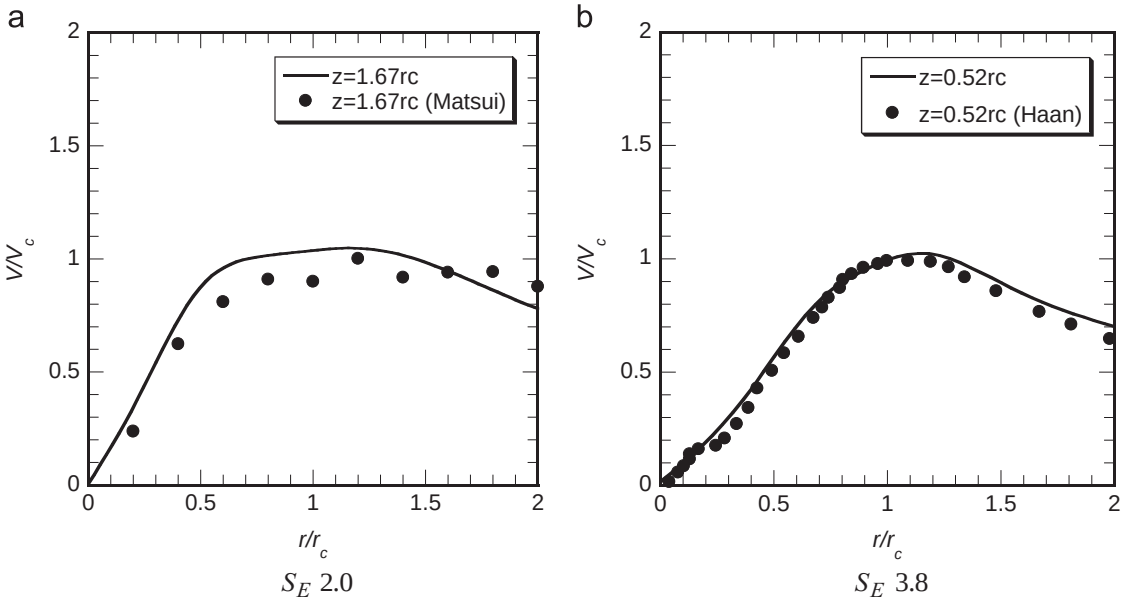

Fig. 8. Comparison of the predicted and measured tangential velocity for (a) touching down stage with $S_E=2.0$ and (b) multi-vortex stage with $S_E=3.8$.

2.6. Modeling roughness

In experimental studies, roughness blocks are employed to consider the effect of rough ground. By modifying the areal density of the blocks, the roughness can be changed. As shown in Eq. (8), a method by adding an appropriate momentum source term in Navier–Stokes equations to numerically simulate the roughness is used in this study:

$$\rho\frac{\partial\tilde{u}_i}{\partial t}+\rho\frac{\partial\tilde{u}_i\tilde{u}_j}{\partial x_j}=\frac{\partial}{\partial x_j}\left(\mu\frac{\partial\tilde{u}_i}{\partial x_j}\right)-\frac{\partial\tilde{p}}{\partial x_i}-\frac{\partial\tau_{ij}}{\partial x_j}+f_{\tilde{u},i} \tag{8}$$

where $f_{\tilde{u},i}$ is the source term for the momentum equation in the i direction and $f_{\tilde{u},i}$ can be calculated as:

$$f_{\tilde{u},i}=-\frac{1}{2}\rho C_{D,\tilde{u}_i}a_{\tilde{u}}\tilde{u}_{mag}\tilde{u}_i \tag{9}$$

where $C_{D,\tilde{u}_i}$ is the drag coefficient of the roughness; $a_{\tilde{u}}$ is the frontal area density, determined by γ_0/h_R; γ_0 is the roughness volume density and h_R is the height of roughness; $\tilde{u}_{mag}$ is the velocity magnitude.

This method is validated through the comparison with the experiment of Maruyama (1993). The schematic of this experiment

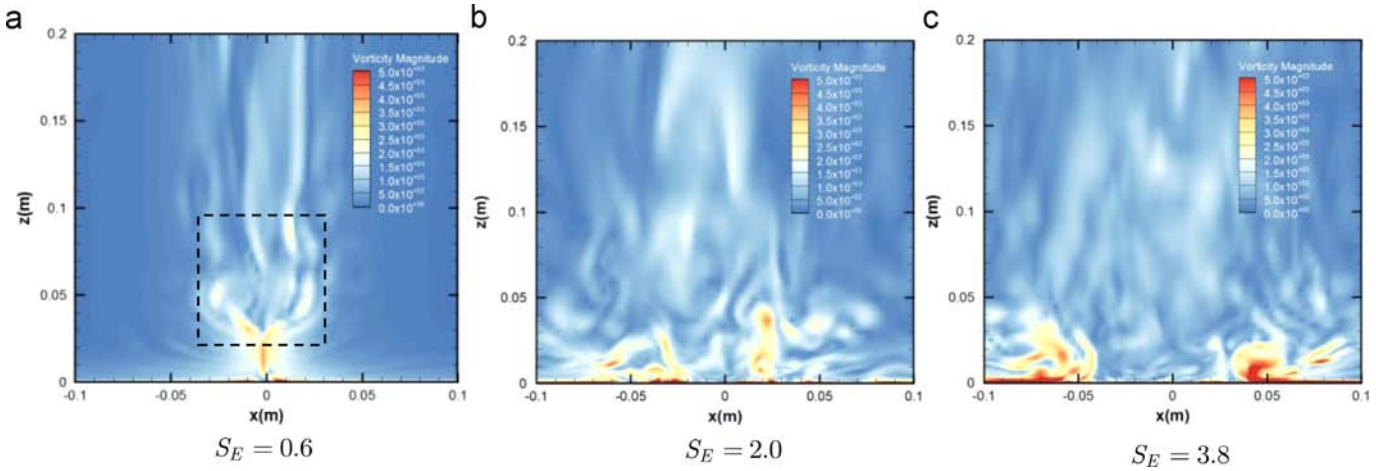

Fig. 9. Contours of instantaneous vorticity magnitude on the vertical cross-section of stationary tornado over smooth ground.

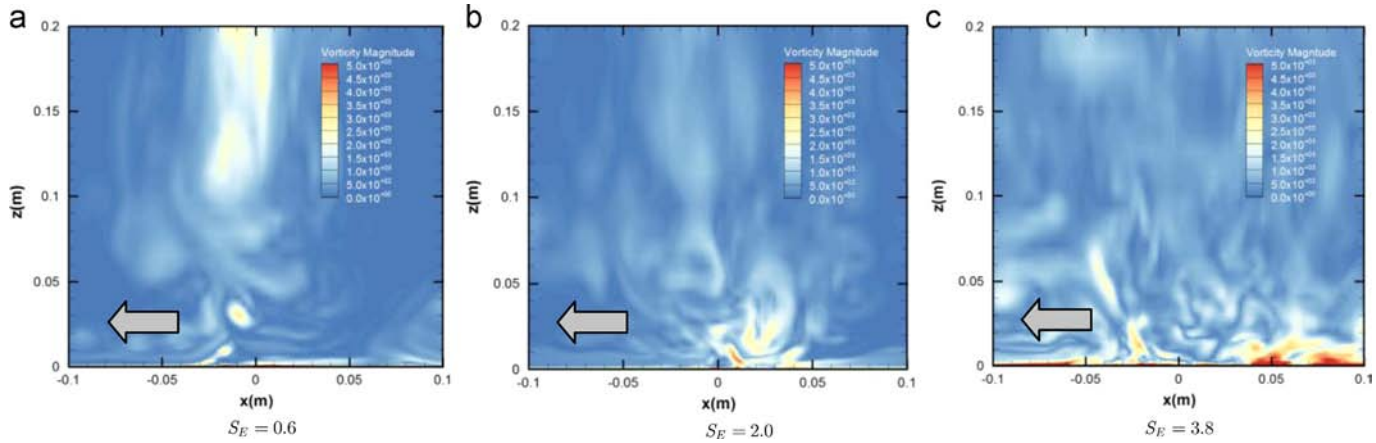

Fig. 10. Contours of instantaneous vorticity magnitude on the vertical cross-section of translating tornado. The arrows indicate the direction of translation of tornado.

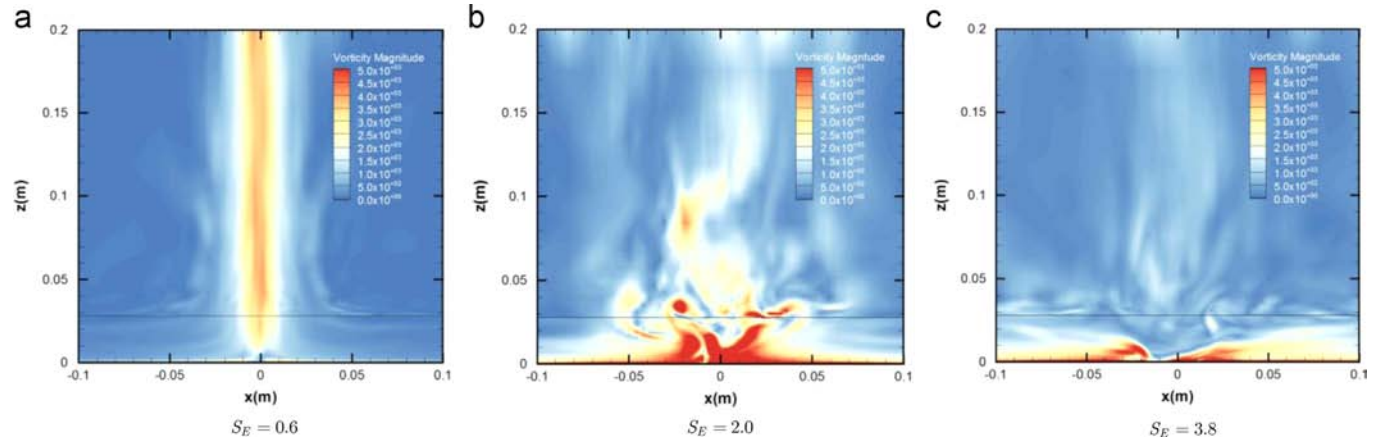

Fig. 11. Contours of instantaneous vorticity magnitude on the vertical cross-section of tornado over rough ground. The solid lines indicate the height of roughness canopy.

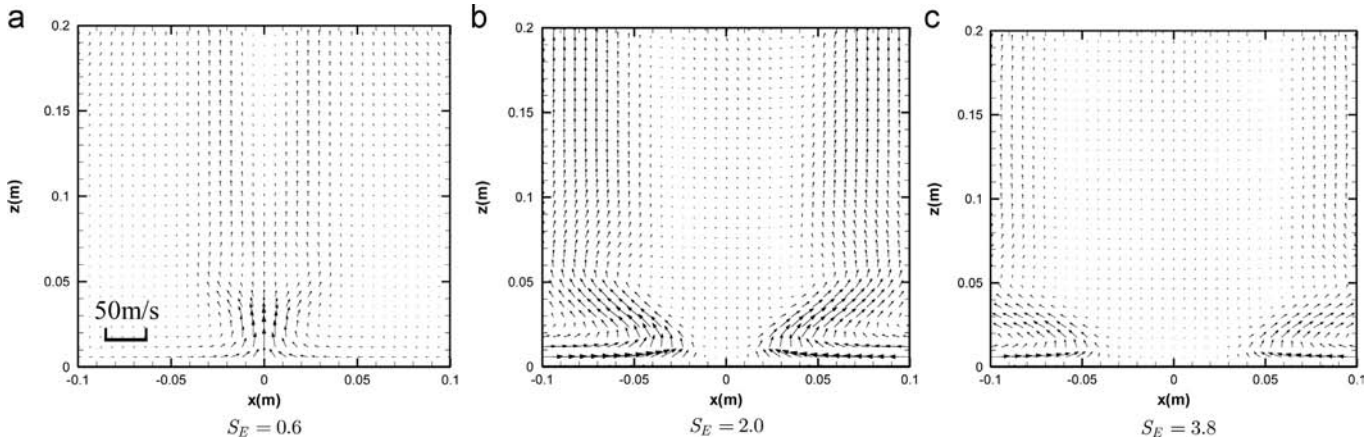

Fig. 12. Vectors of time averaged flow fields on the vertical cross-section of stationary tornado over smooth ground.

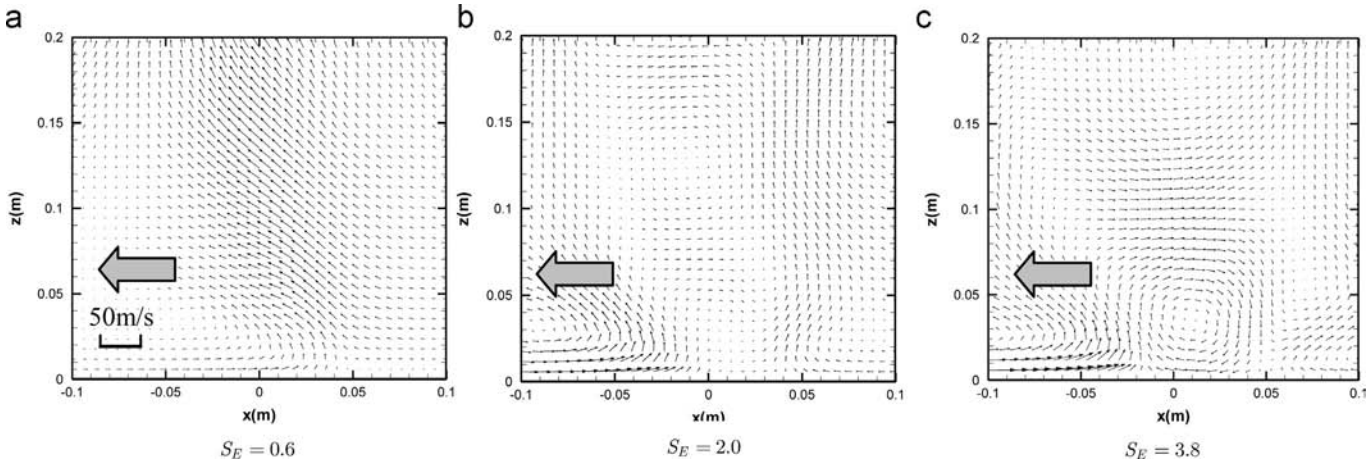

Fig. 13. Vectors of time averaged flow fields on the vertical cross-section of translating tornado. The big arrows indicate the translation of tornado.

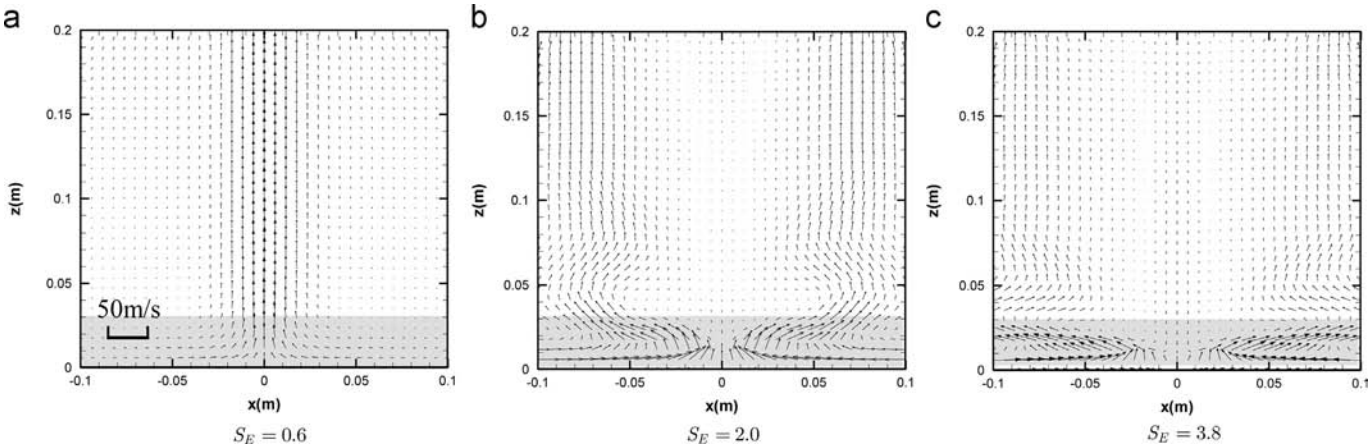

Fig. 14. Vectors of time averaged flow fields on the vertical cross-section of tornado over rough ground. The gray shaded areas indicate the roughness canopy.

is shown in Fig. 4. The roughness block size is 0.03 m × 0.03 m, the roughness volume density γ_0 was set as 5.6%, 12.5% and 25%. Inflow wind speed is set as 1 m/s uniformly. The drag coefficients in x, y and z directions are respectively 2.0, 2.0 and 0.0. In the z direction there is no drag effect from the roughness blocks, that is why 0.0 is used for $C_{D,\tilde{u}_z}$.

Figs. 5 and 6 show mean wind speed and the kinetic energy at the location of x=12.95 m. Satisfactory agreement with the data from the experiment by Maruyama (1993) indicates that the roughness effects can successfully be simulated by adding an appropriate momentum source term in the Navier–Stokes equations for the boundary layer flow.

In the present study about tornado over ground roughness, according to the study of Zhang and Sarkar (2008) and Matsui and Tamura (2009), only uniform roughness blocks are considered. Uniform roughness blocks have a volume density γ_0 of 0.056.

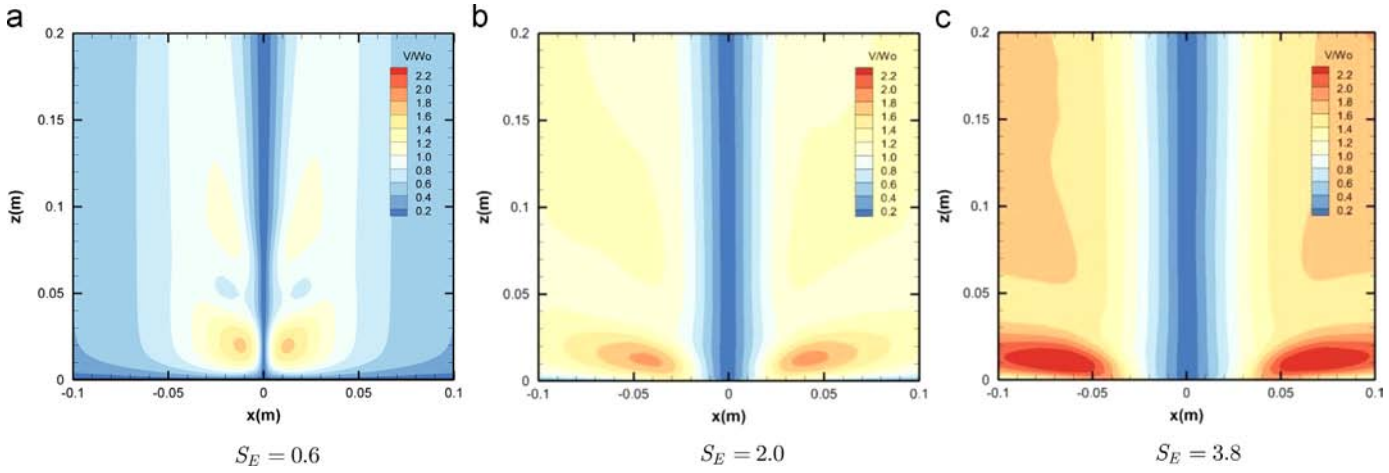

Fig. 15. Contours of time averaged tangential velocity on the vertical cross-section of stationary tornado over smooth ground.

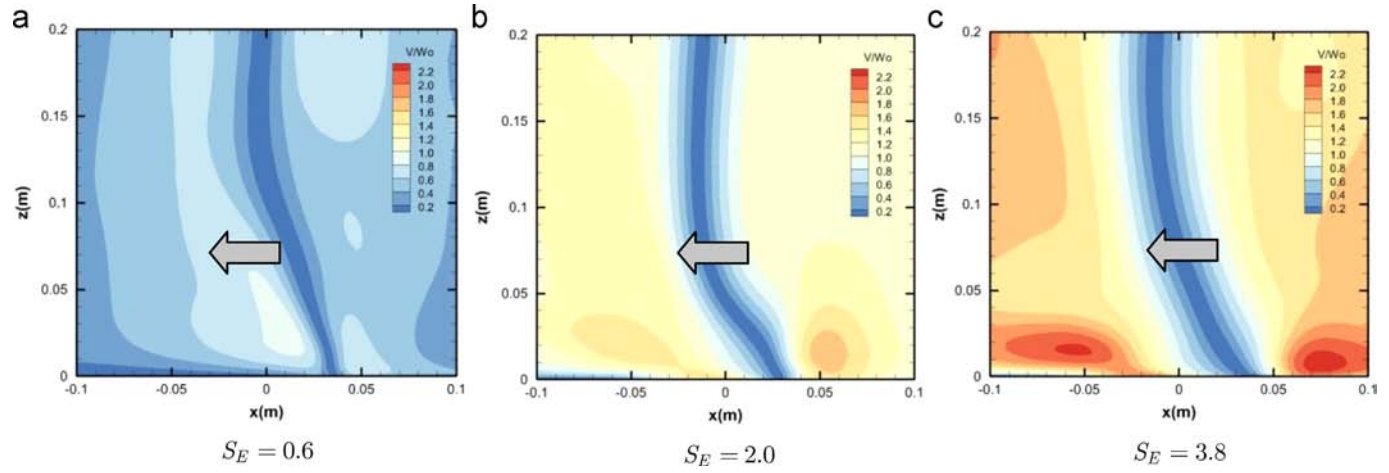

Fig. 16. Contours of time averaged tangential velocity on the vertical cross-section of translating tornado. The arrows indicate the direction of translation of tornado.

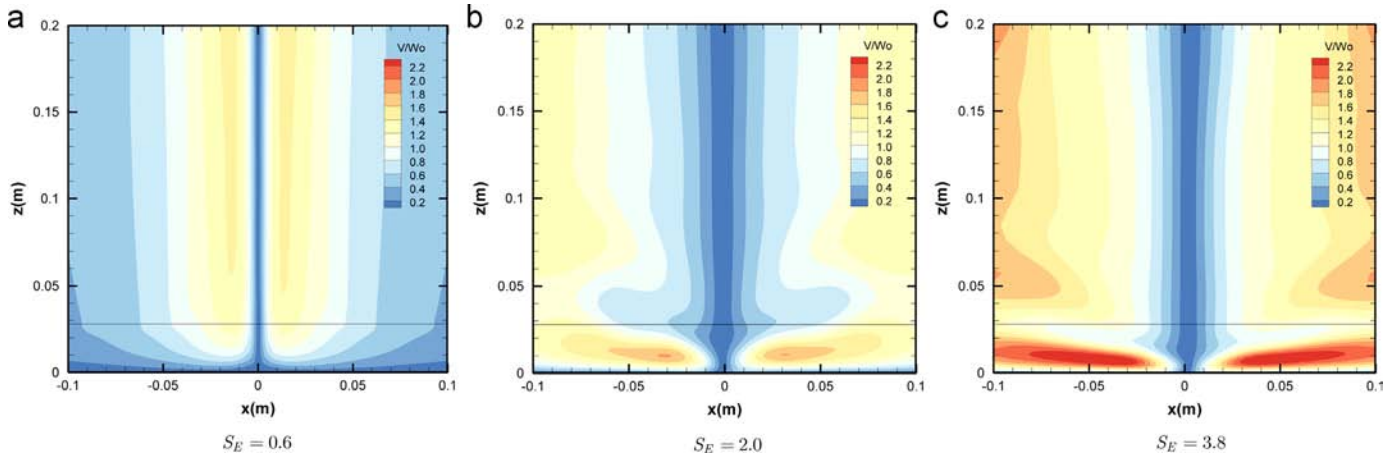

Fig. 17. Contours of time averaged tangential velocity on the vertical cross-section of tornado over rough ground. The solid lines indicate the height of roughness canopy.

Consistent with the above validation $C_{D,\tilde{u}_x}$, $C_{D,\tilde{u}_y}$ and $C_{D,\tilde{u}_z}$ are respectively determined as 2.0, 2.0 and 0.0. The height of the roughness, h_R, is decided as 0.026 m. Considering that the length scale of the simulator is 1:1905 as to be introduced in the following discussion, the roughness height is 50 m in full scale, which corresponds to the central city. As shown in Fig. 7(a), the roughness region has a radius of 0.6 m which begins at the location of 0.4 m from the inlet. Uniform roughness blocks are ideal, however only this ideal case is expected to be examined in the present study, so as to shed some lights on the effects of ground roughness on tornado-like vortices. In the future, researches considering non-uniform roughness blocks or roughness blocks with other volume densities will be carried out. Applied in the present study, the method simulating roughness blocks has

Table 8
Numerical results of the representative dimensional parameters.

	Case name	V_c (m/s)	r_c (m)	U_{min} (m/s)	V_{max} (m/s)	W_{max} (m/s)	$r_{v\ max}$ (m)	$h_{v\ max}$ (m)	P_{min} (Pa)
Stationary tornado over smooth ground	Case1	10.7	0.014	–	–	–	–	–	−5
	Case2	9.8	0.024	−10.6	15.7	25.3	0.013	0.020	−106
	Case3	9.1	0.035	−8.6	12.2	10.1	0.021	0.016	−205
	Case4	9.6	0.047	−9.2	13.0	6.2	0.027	0.015	−216
	Case5	11.0	0.054	−9.6	13.7	6.0	0.035	0.014	−339
	Case6	12.4	0.073	−11.1	17.1	5.7	0.043	0.013	−410
	Case7	14.3	0.084	−11.8	19.0	4.7	0.055	0.012	−509
	Case8	16.0	0.097	−13.7	21.8	4.7	0.058	0.011	−619
	Case9	18.6	0.112	−15.9	26.6	5.0	0.063	0.010	−674
Translating tornado	Case1.t	11.1	0.013	–	–	–	–	–	−19
	Case2.t	7.8	0.021	−6.2	10.4	6.5	0.011	0.024	−41
	Case3.t	9.6	0.032	−6.7	10.2	5.0	0.021	0.018	−82
	Case4.t	9.5	0.041	−8.1	11.8	5.9	0.029	0.012	−115
	Case5.t	11.3	0.062	−10.2	14.9	5.6	0.045	0.017	−228
	Case6.t	13.2	0.074	−11.6	17.3	6.2	0.045	0.015	−331
	Case7.t	15.4	0.082	−13.5	20.5	7.2	0.060	0.011	−440
	Case8.t	16.3	0.097	−14.1	21.7	7.3	0.056	0.010	−505
	Case9.t	17.3	0.120	−15.3	23.3	7.2	0.068	0.010	−581
Tornado over rough ground	Case1.r	13.1	0.010	–	–	–	–	–	−21
	Case2.r	12.6	0.014	–	–	–	–	–	−50
	Case3.r	9.6	0.043	−11.3	16.3	23.1	0.010	0.021	−95
	Case4.r	10.1	0.057	−13.6	20.8	33.8	0.012	0.022	−158
	Case5.r	10.7	0.086	−12.2	14.8	7.2	0.026	0.013	−197
	Case6.r	12.1	0.092	−13.5	17.4	7.2	0.031	0.011	−286
	Case7.r	14.4	0.096	−15.9	20.5	6.8	0.046	0.012	−429
	Case8.r	14.8	0.098	−16.0	20.9	5.7	0.052	0.011	−466
	Case9.r	15.8	0.108	−17.5	23.2	5.3	0.053	0.011	−569

*Simple "–" means the data is not available in the simulation.

Table 9
Numerical results of the representative nondimensional parameters.

	Case name	V_{max}/v_T	$-U_{max}/v_T$	h_{vmax}/h_R	V_{max}/V_c	$-U_{min}/V_c$	W_{max}/V_{max}	$r_{v\ max}/h_{v\ max}$
Stationary tornado over smooth ground	Case1	–	–	–	–	–	–	–
	Case2	–	–	–	1.60	−1.08	1.61	0.65
	Case3	–	–	–	1.34	−0.95	0.83	1.31
	Case4	–	–	–	1.35	−0.96	0.48	1.80
	Case5	–	–	–	1.25	−0.87	0.44	2.50
	Case6	–	–	–	1.38	−0.90	0.33	3.31
	Case7	–	–	–	1.33	−0.83	0.25	4.58
	Case8	–	–	–	1.36	−0.86	0.22	5.27
	Case9	–	–	–	1.43	−0.85	0.19	6.30
Translating tornado	Case1.t	–	–	–	–	–	–	–
	Case2.t	3.15	1.88	–	1.33	−0.79	0.63	0.46
	Case3.t	3.09	2.03	–	1.06	−0.70	0.49	1.17
	Case4.t	3.58	2.45	–	1.24	−0.85	0.50	2.42
	Case5.t	4.52	3.09	–	1.32	−0.90	0.38	2.65
	Case6.t	5.24	3.52	–	1.31	−0.88	0.36	3.00
	Case7.t	6.21	4.09	–	1.33	−0.88	0.35	5.45
	Case8.t	6.58	4.27	–	1.33	−0.87	0.34	5.60
	Case9.t	7.06	4.64	–	1.35	−0.88	0.31	6.80
Tornado over rough ground	Case1.r	–	–	–	–	–	–	–
	Case2.r	–	–	–	–	–	–	–
	Case3.r	–	–	0.81	1.70	−1.18	1.42	0.48
	Case4.r	–	–	0.85	2.06	−1.35	1.63	0.55
	Case5.r	–	–	0.50	1.38	−1.14	0.49	2.00
	Case6.r	–	–	0.42	1.44	−1.12	0.41	2.82
	Case7.r	–	–	0.46	1.42	−1.10	0.33	3.83
	Case8.r	–	–	0.42	1.41	−1.08	0.27	4.73
	Case9.r	–	–	0.42	1.47	−1.11	0.23	4.82

*Simple "–" means the data is not available in the simulation.

been adopted in a large number of researches concerning the straight line boundary layer flow, which also has x, y and z velocity components and provides accurate results. For the typhoon case, it is relative to determine a flow is swirling or not. It is swirling from large scale view and flow fields also have three velocity components. For this kind of flow, the method adopted in this study is classic to consider the surface roughness. Therefore, it can be safely said that the method applied in this study to consider the surface roughness is applicable for tornado-like vortices as well, even this method is used in the tornado like flow for the first time. Parameters modeling the tornado over rough ground are listed in Table 6.

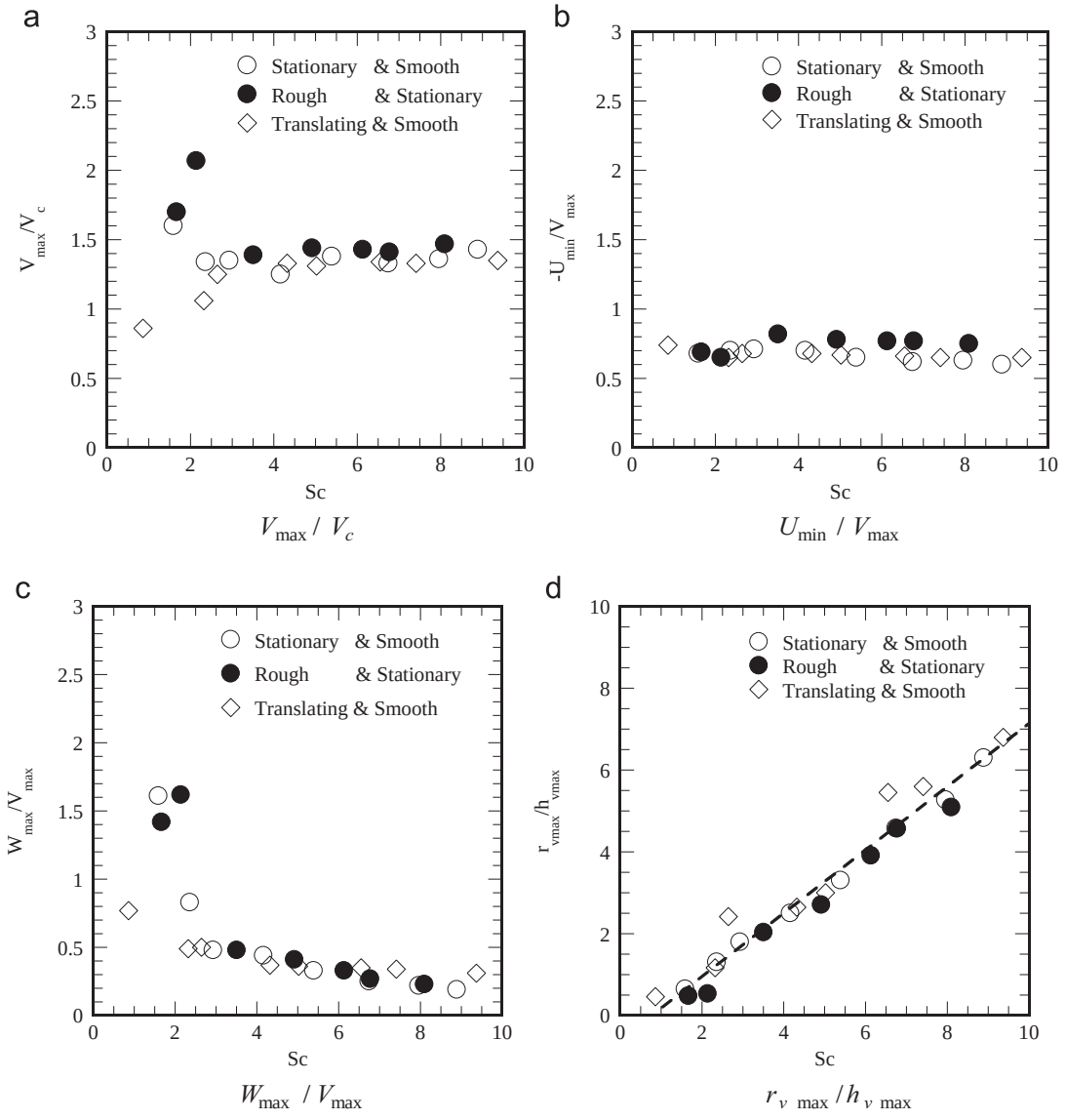

Fig. 18. Summery of surface intensification and the geometry of tornado vortices as a function of local corner swirl ratio.

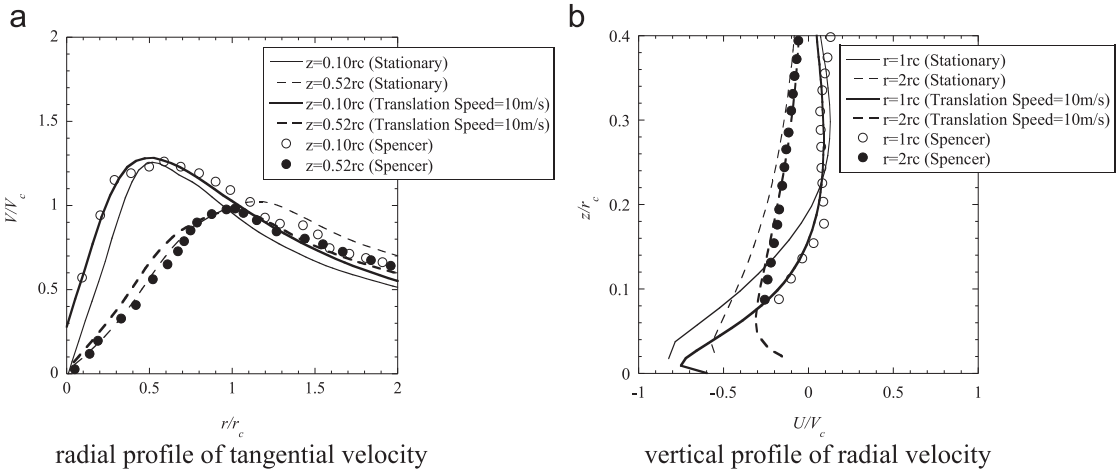

Fig. 19. Comparison of stationary tornado, translating tornado and Spencer tornado.

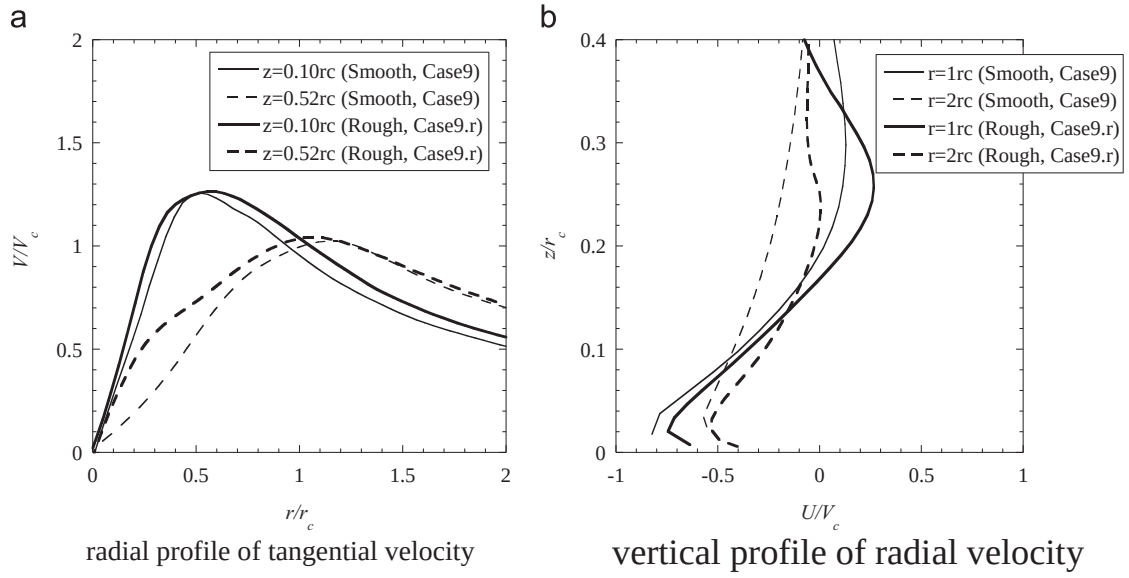

Fig. 20. Comparison of the tornado over smooth and rough ground.

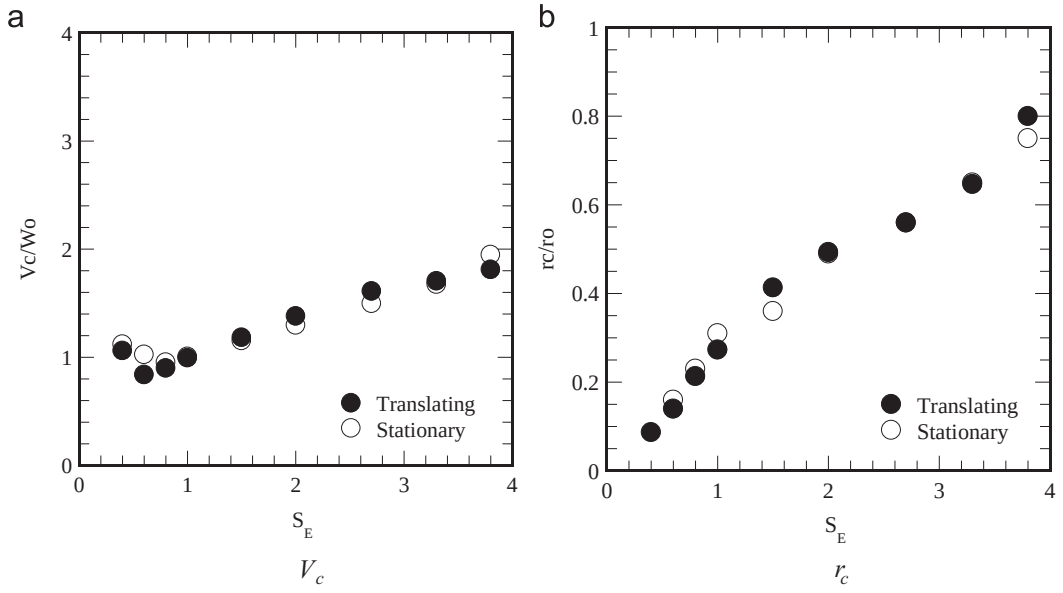

Fig. 21. Comparison of (a) V_c and (b) r_c between translating and stationary tornados.

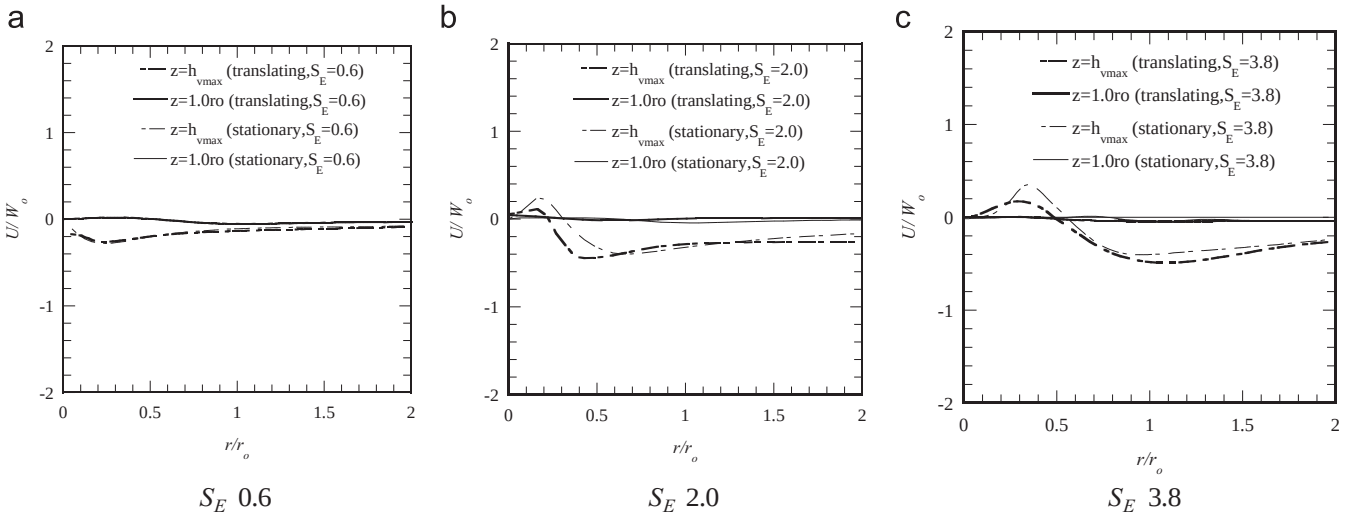

Fig. 22. Comparison of radial profiles of the radial velocity between translating and stationary tornados.

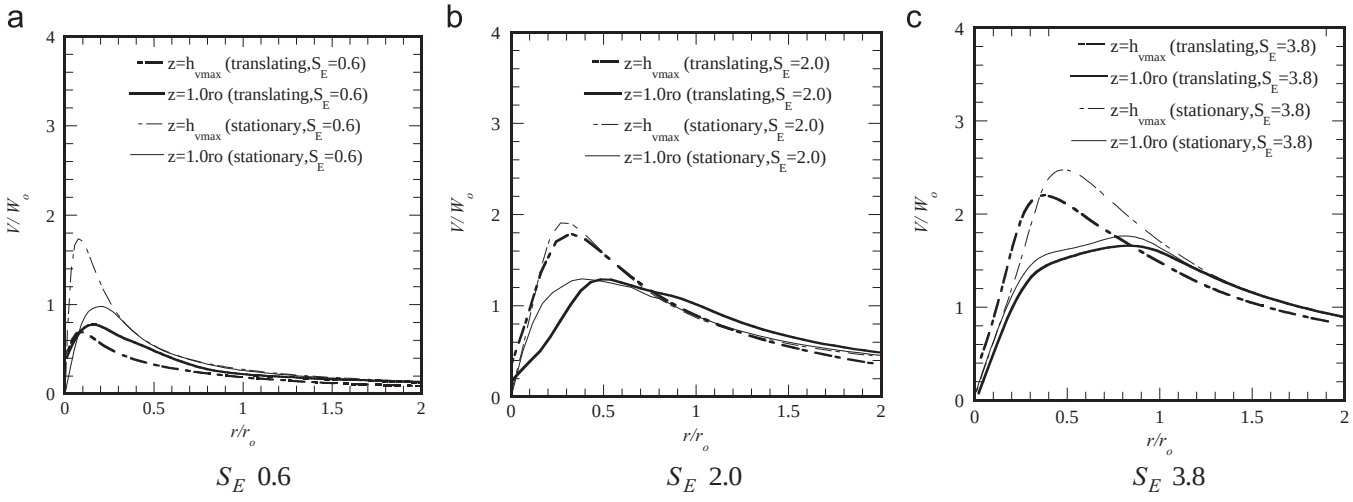

Fig. 23. Comparison of radial profiles of the tangential velocity between translating and stationary tornados.

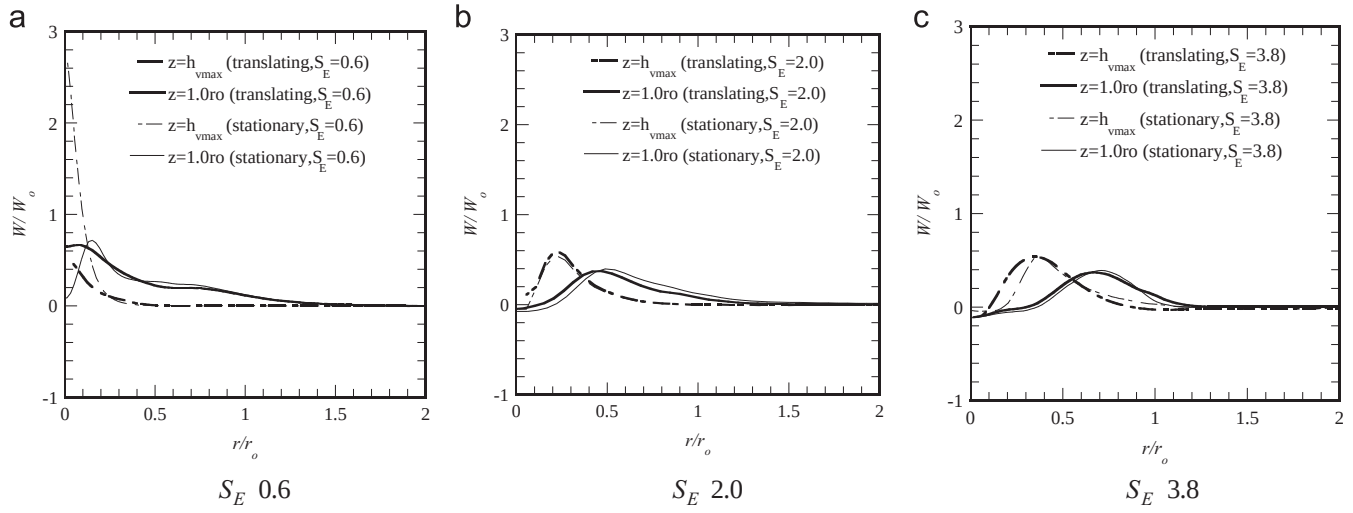

Fig. 24. Comparison of radial profiles of the vertical velocity between translating and stationary tornados.

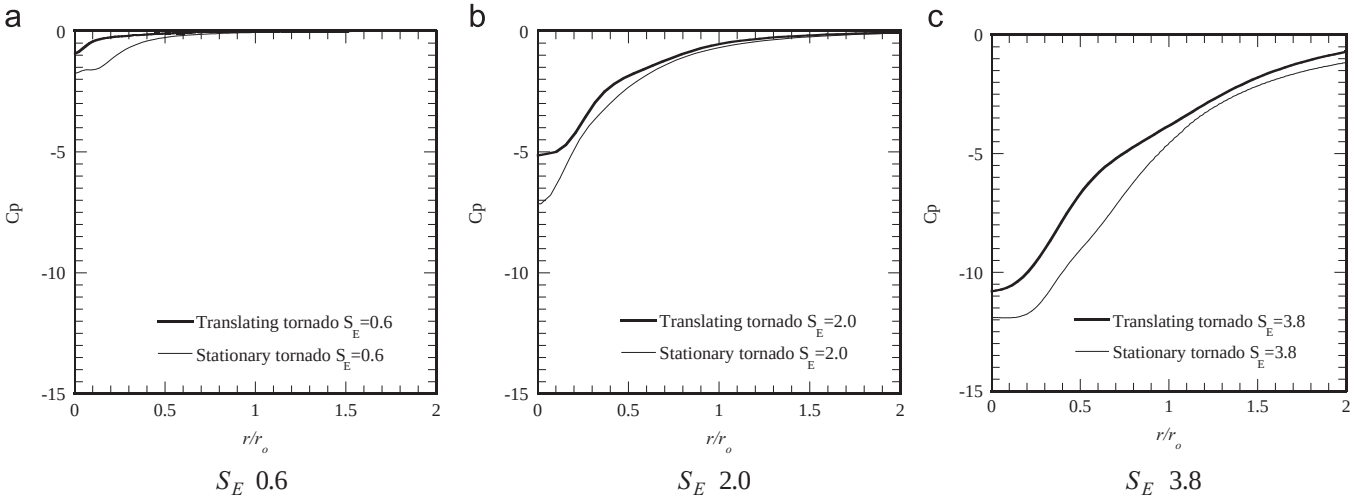

Fig. 25. Comparison of radial profiles of the pressure coefficient between translating and stationary tornados.

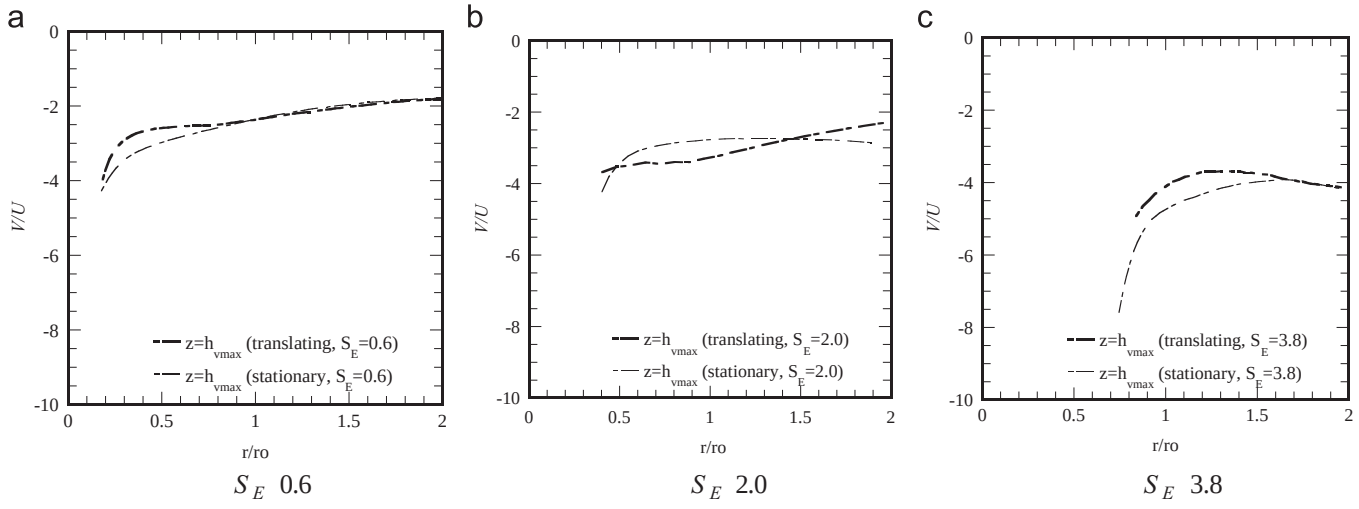

Fig. 26. Comparison of radial profiles of V/U at $z = h_{v\ max}$ between translating and stationary tornados.

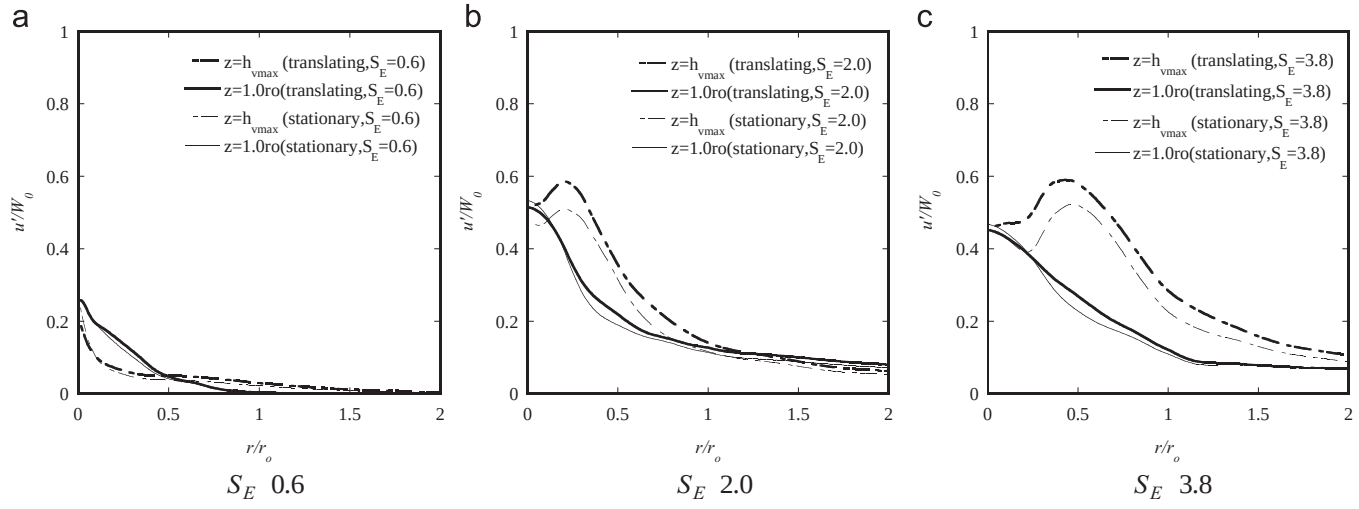

Fig. 27. Comparison of radial profiles of the radial fluctuations between translating and stationary tornados.

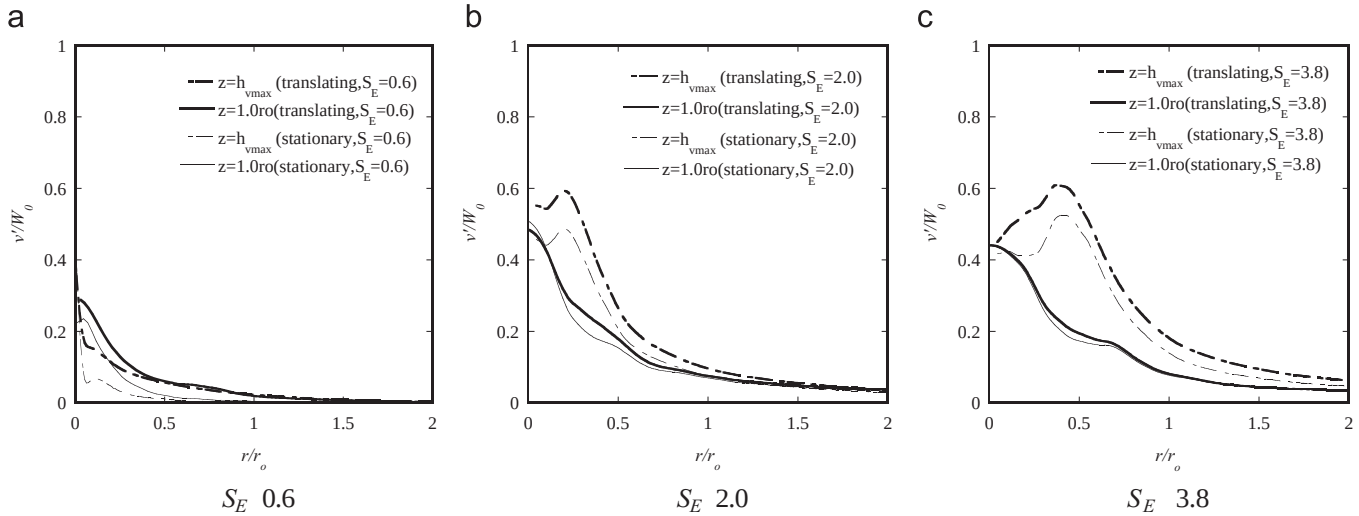

Fig. 28. Comparison of radial profiles of the tangential fluctuations between translating and stationary tornados.

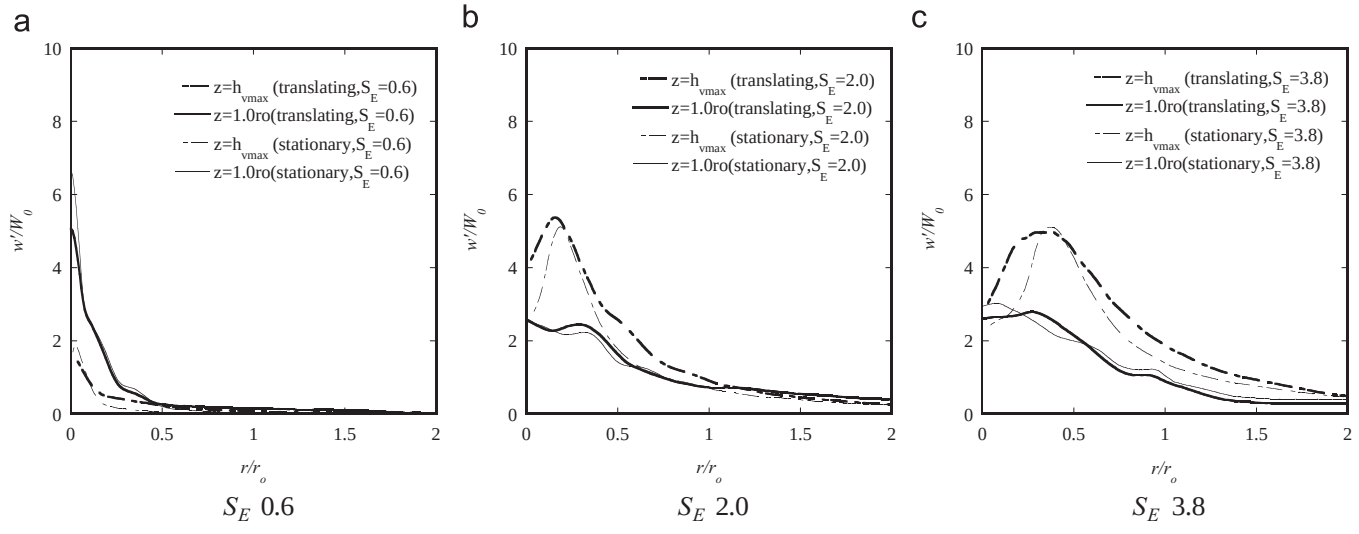

Fig. 29. Comparison of radial profiles of the vertical fluctuations between translating and stationary tornados.

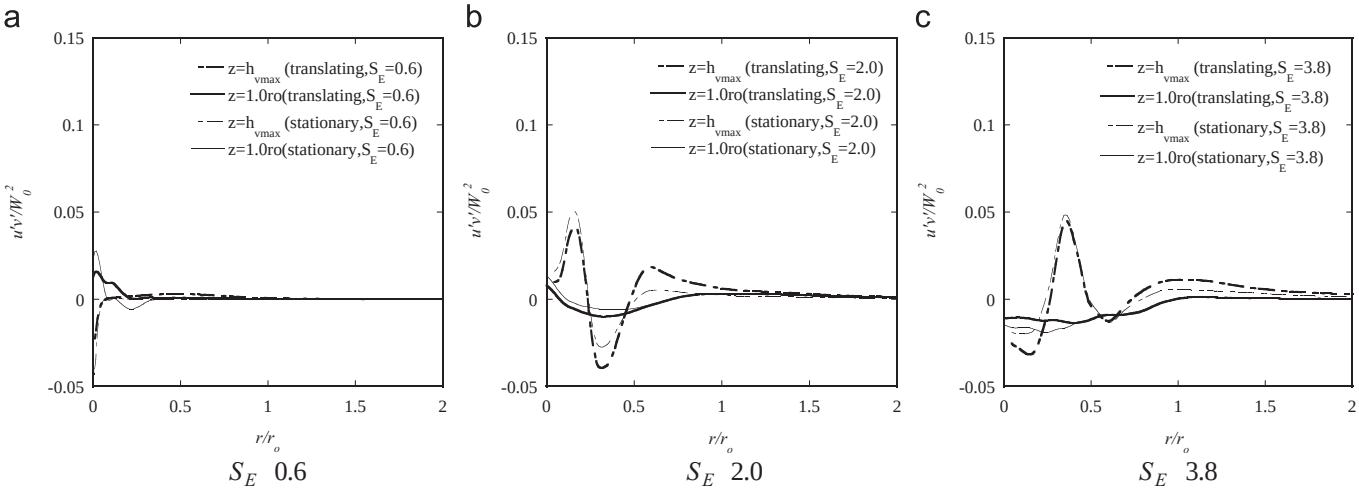

Fig. 30. Comparison of radial profiles of the Reynolds shear stress *u*'*v*' between translating and stationary tornados.

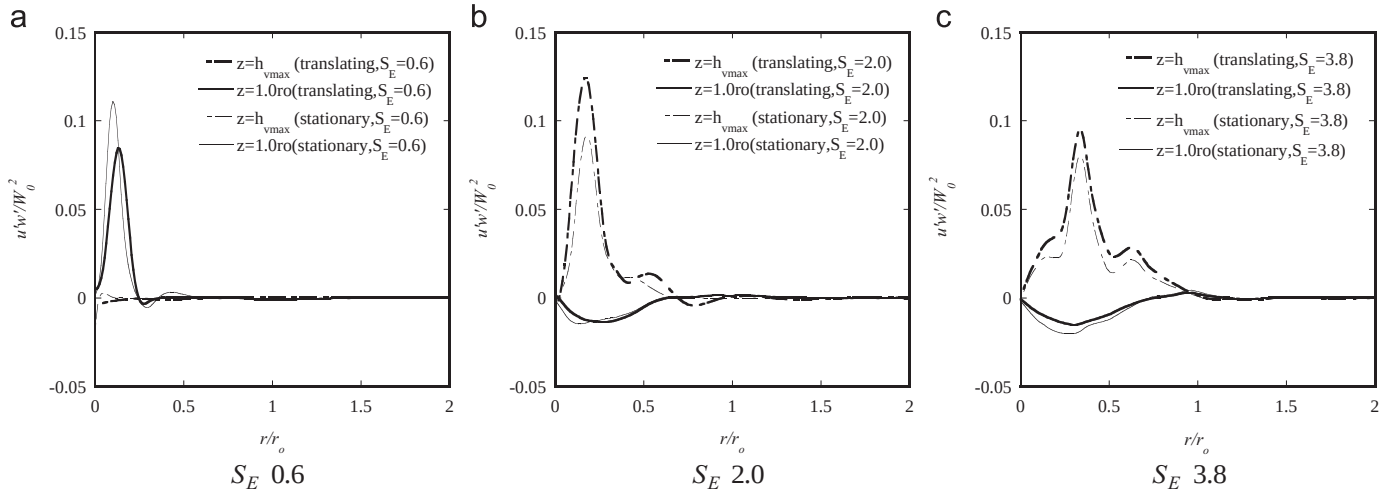

Fig. 31. Comparison of radial profiles of the Reynolds shear stress *u*'*w*' between translating and stationary tornados.

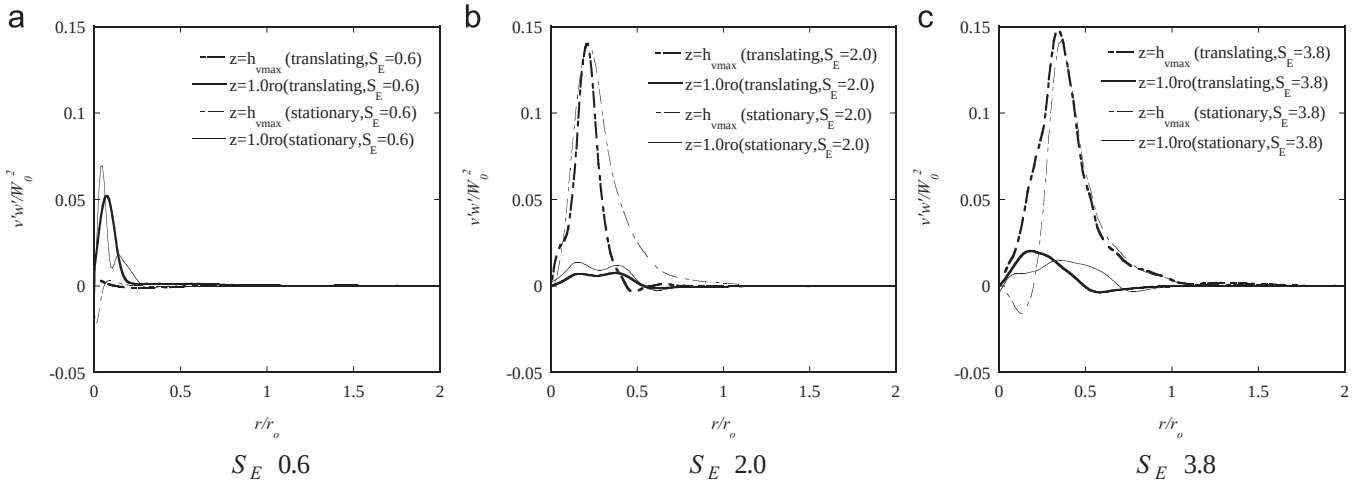

Fig. 32. Comparison of radial profiles of the Reynolds shear stress $v'w'$ between translating and stationary tornados.

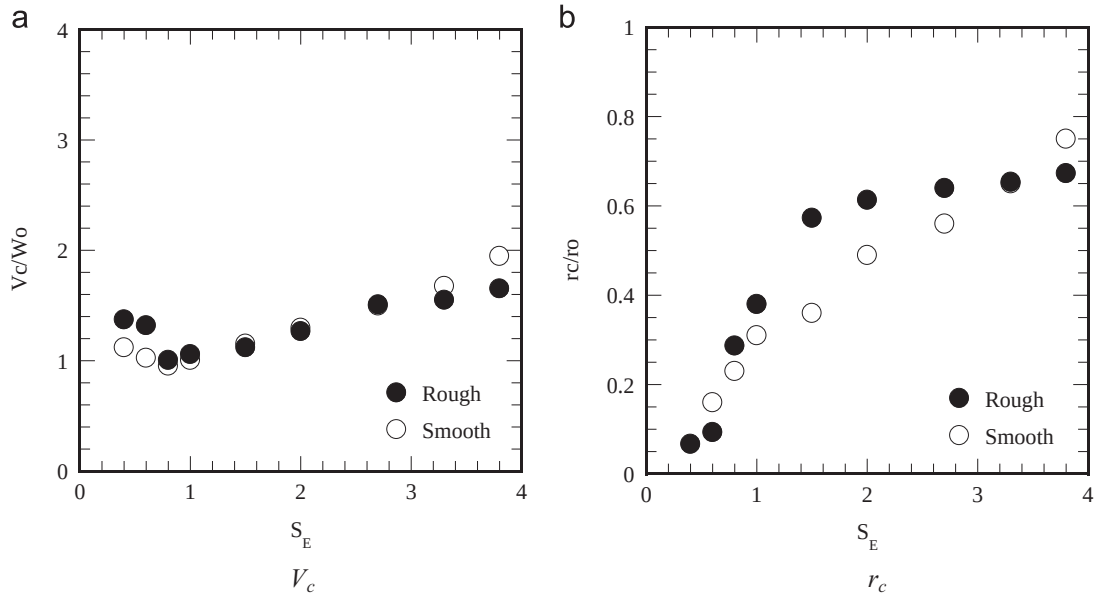

Fig. 33. Comparison of normalized V_c and r_c between tornados over rough and smooth grounds.

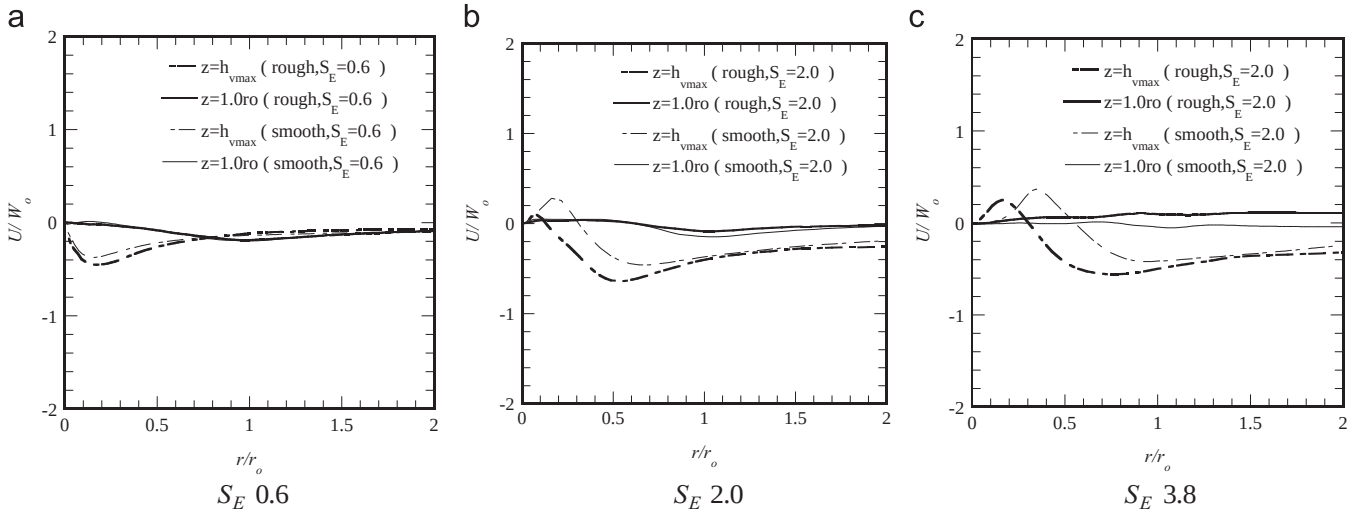

Fig. 34. Comparison of radial profiles of the radial velocity between tornados over rough and smooth grounds.

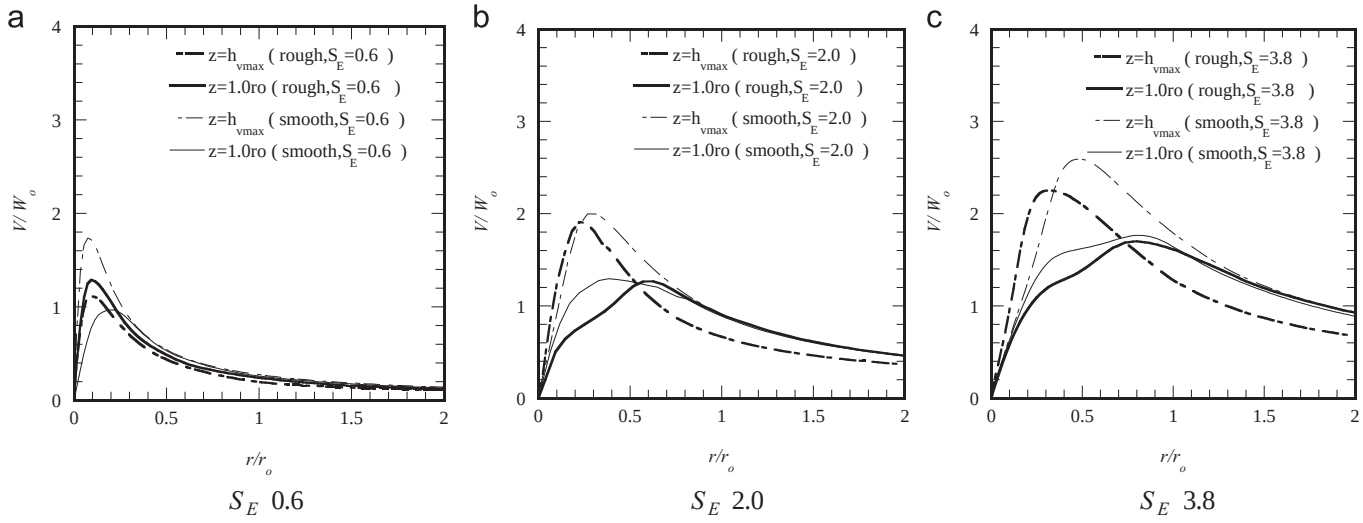

Fig. 35. Comparison of radial profiles of the tangential velocity between tornado over rough ground and that over smooth ground.

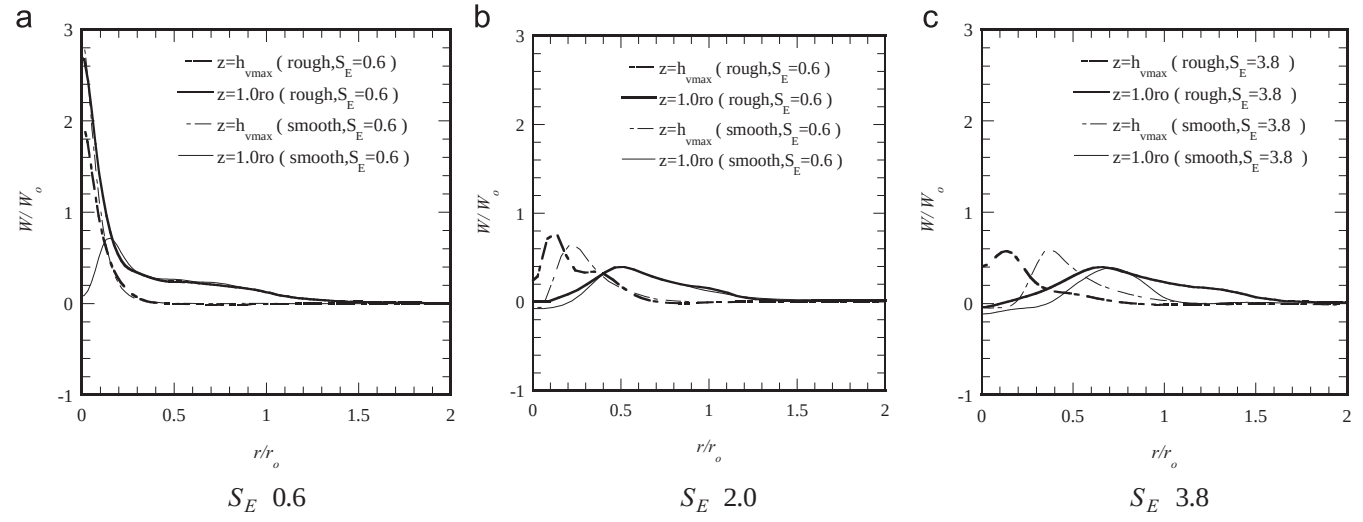

Fig. 36. Comparison of radial profiles of the vertical velocity between tornados over rough and smooth grounds.

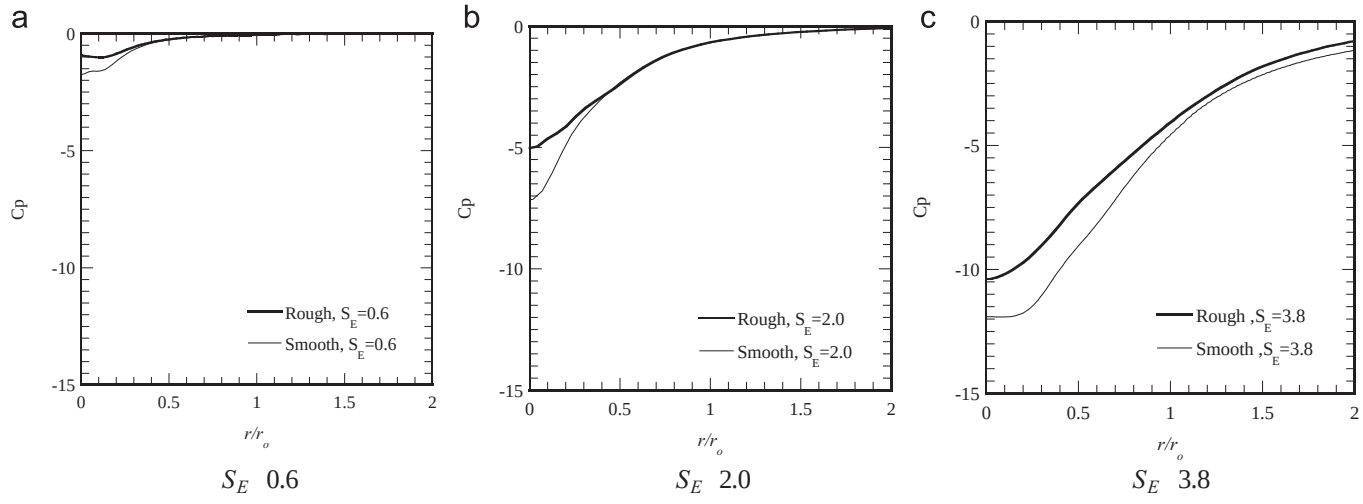

Fig. 37. Comparison of radial profiles of pressure coefficient between tornados over rough and smooth grounds.

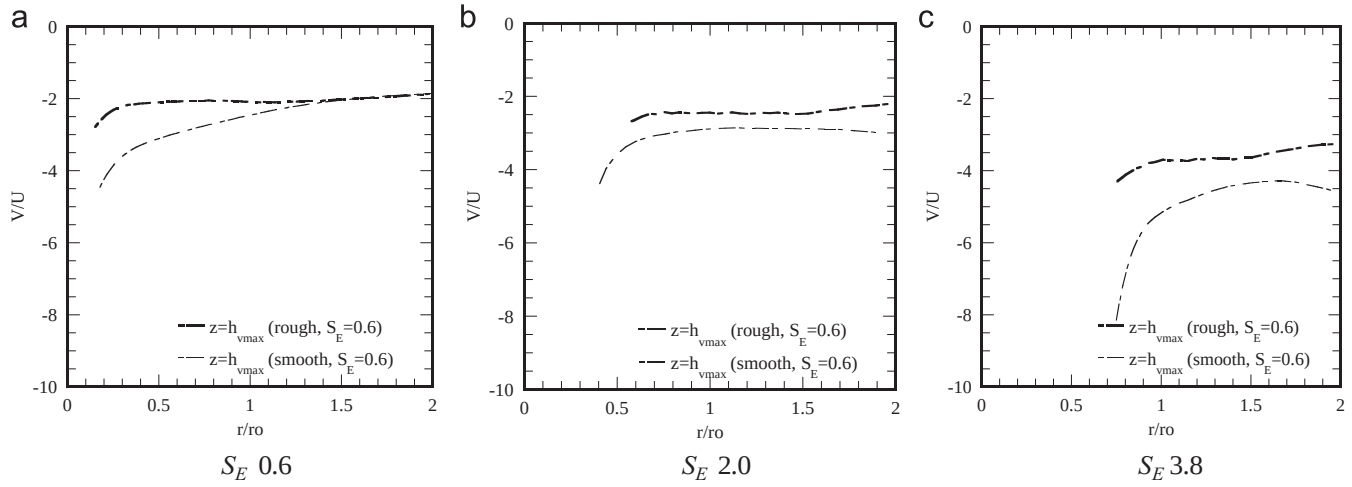

Fig. 38. Comparison of radial profiles of V/U at $z = h_{v\ max}$ between tornados over rough and smooth grounds.

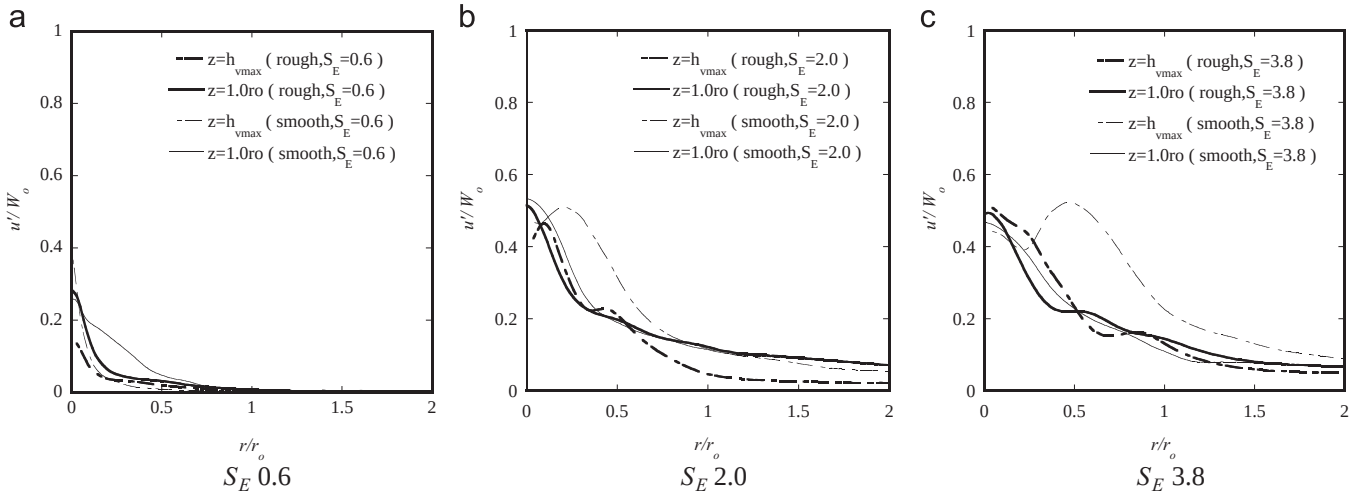

Fig. 39. Comparison of radial profiles of the radial fluctuations between tornado over rough ground and that over smooth ground.

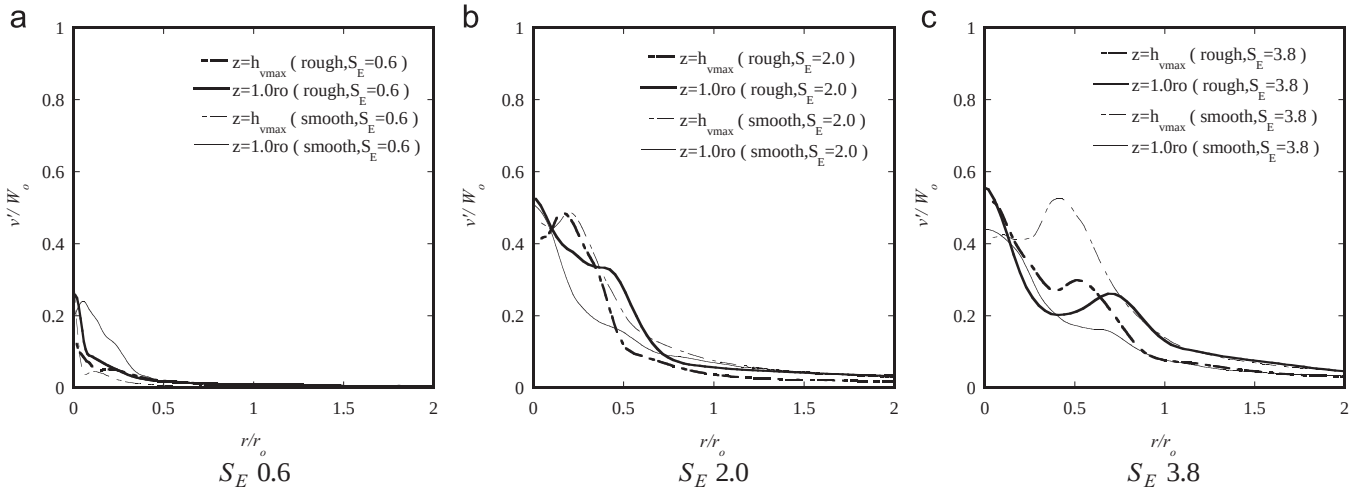

Fig. 40. Comparison of radial profiles of the tangential fluctuations between tornado over rough ground and that over smooth ground.

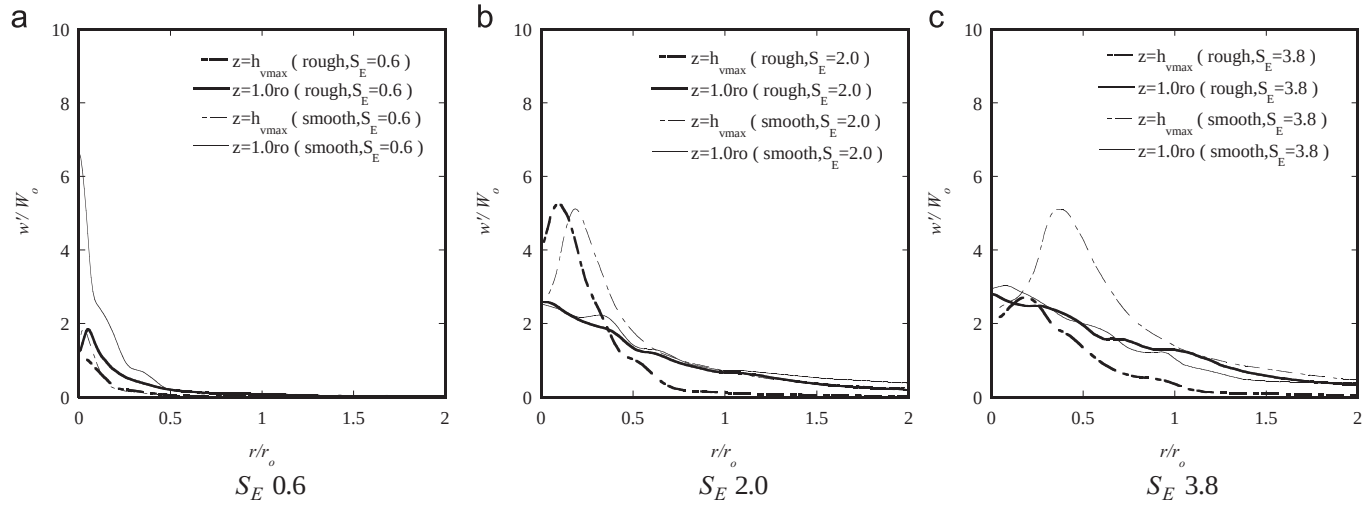

Fig. 41. Comparison of radial profiles of the vertical fluctuations between tornado over rough ground and that over smooth groud.

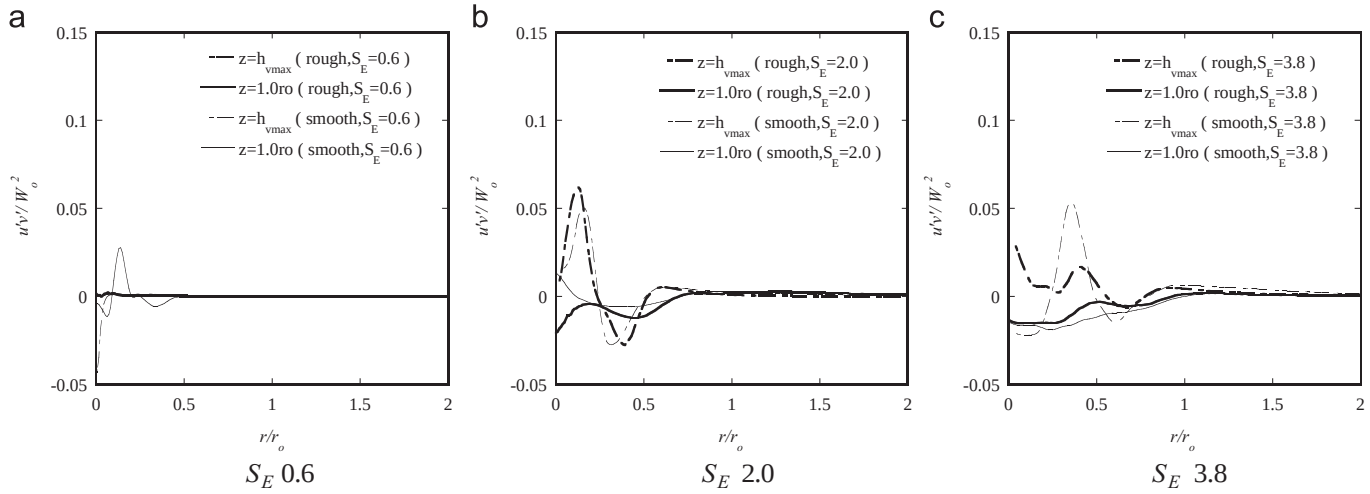

Fig. 42. Comparison of radial profiles of the Reynolds shear stress $u'v'$ between tornado over rough ground and that over smooth ground.

2.7. Definitions of swirl ratio

For experimental simulators by Church et al. (1979), Monji (1985), Mishra et al. (2008), and Tari et al. (2010) as well as numerical simulators by Rotunno (1977), Wilson and Rotunno (1986) and Ishihara et al. (2011), the external swirl ratio has historically been defined as the ratio of angular momentum to radial momentum in the vortex, and expressed as follows:

$$S_E = \frac{\Gamma_\infty}{2Qh/r_0} = \frac{\tan\theta}{2a} \tag{10}$$

where Γ_∞ is the circulation at the outer edge of the convergent region, $\Gamma_\infty = 2\pi r_s h V_{rs}$, and a is the aspect ratio, $a = h/r_0$, h and r_0 are the height of the inlet layer and the radius of the updraft hole, respectively.

In the study by Lewellen et al. (2000), the local corner swirl ratio, S_c, is expressed as:

$$S_c = \frac{r_c^* \Gamma_\infty^{*\,2}}{\Upsilon} \tag{11}$$

where r_c^* is the characteristic length scale and calculated as $r_c^* \equiv \Gamma_\infty^*/V_c$. V_c is the maximum tangential velocity in the cyclostrophic balance region, same as the study by Liu and Ishihara (2015a) and determined at $z = 1.0r_0$. The circulation per unit height in the outer region is expressed as $\Gamma_\infty^* = V(r_2, z_2)r_2$ and the total depleted circulation flux flowing through the corner flow region, Υ, is expressed as:

$$\Upsilon \approx 2\pi \int_0^{r_2} W(r, z_2)\ \Gamma_d(r, z_2) r dr \tag{12}$$

where $\Gamma_d(r, z_2) = V(r_2, z_2)r_2 - V(r, z_2)r$ is the depleted angular momentum, where r_2 is a radius safely outside of the upper-core region and z_2 is a height just above the corner flow, as mentioned by Lewellen et al. (2000).

2.8. Case settings

The case settings and parameters are listed in Table 7. In this study, 9 cases are considered for each group. The flow pattern from the single-celled vortex (S_E=0.4) to the vortex touch-down (S_E=0.6) is very sensitive to the change of the swirl ratio. Therefore in order to capture the typical types of tornado from the single-celled vortex to the vortex touch-down, the external swirl ratio increases at a small step size of 0.2. After vortex touch-down, the flow pattern becomes similar, therefore larger step sizes are used and when S_E=3.8 the flow fields become comparable with the Spencer tornado as shown in the following discussion. Among 9 cases in each group, several representative cases are chosen to do detailed examination. The introduction of roughness disturbs the flow fields of tornado obviously at stages of vortex breakdown,

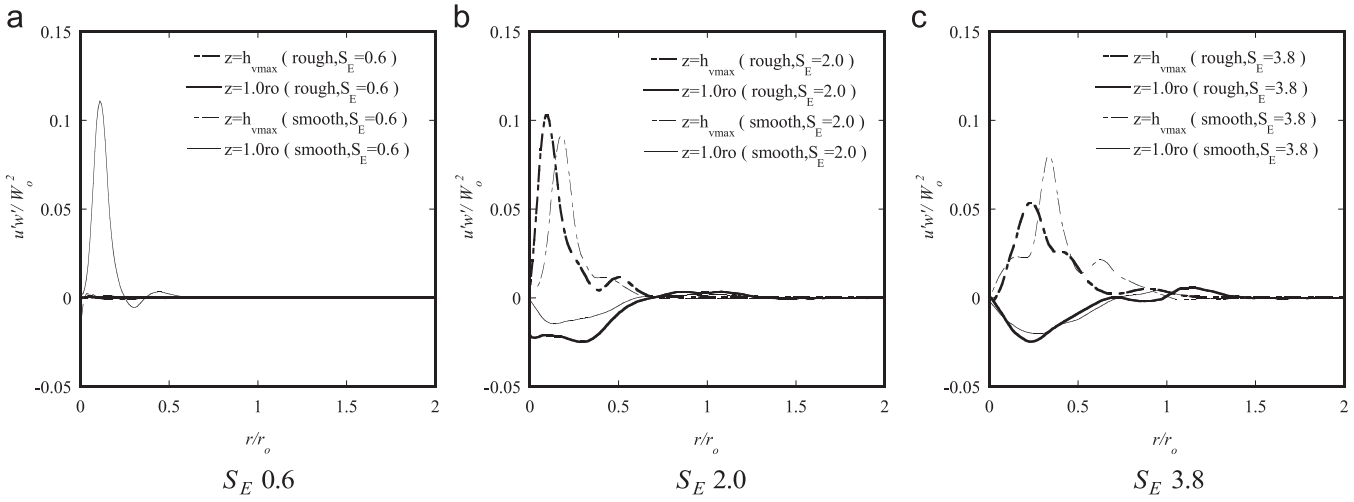

Fig. 43. Comparison of radial profiles of the Reynolds shear stress *u'w'* between tornado over rough ground and that over smooth ground.

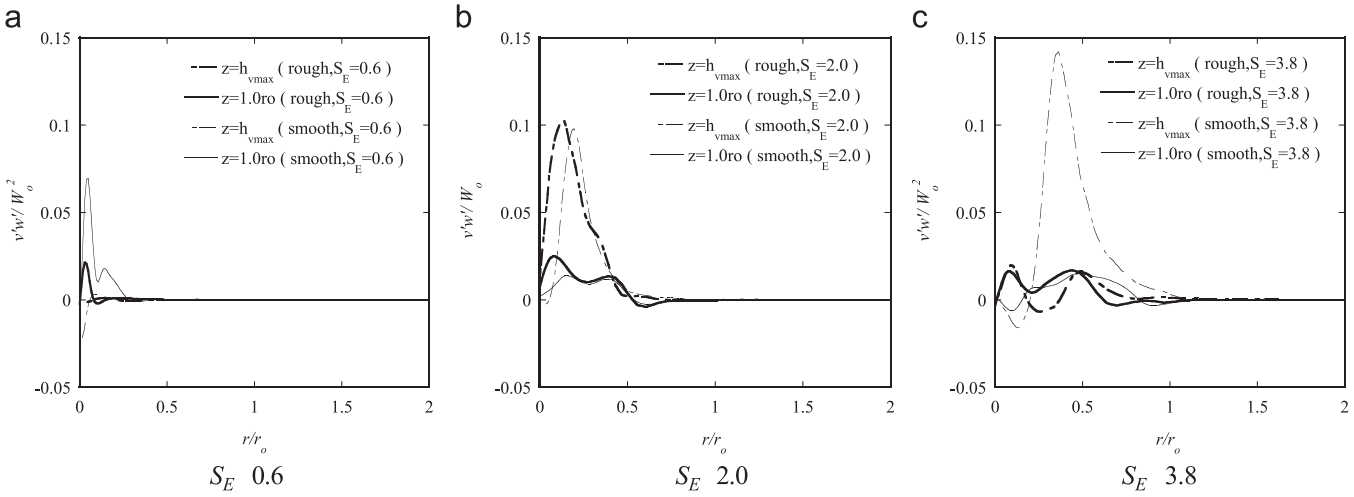

Fig. 44. Comparison of radial profiles of the Reynolds shear stress *v'w'* between tornado over rough ground and that over smooth ground.

Case2, and vortex touching down, Case5. The multi-vortex stage, Case9, corresponds to the Spencer tornado. Therefore, these three representative cases, Case2, Case5, and Case9, are investigated in detail. The subscripts "*.t*" and "*.r*" are used to distinguish the translating tornadoes and the tornadoes over rough ground respectively.

3. Overview of the effects from tornado translation and ground roughness

In this section, the results of the stationary tornadoes over smooth ground are firstly compared with the experiments data to verify the accuracy of the numerical simulator. Then, the flow fields are visualized using vectors and velocity contours. The overall parameters of tornado-like vortices with translation and ground roughness effects are examined to provide a general image on the tornado translation and ground roughness effects. At last the similarity of the tornados with different ground conditions is summerized.

3.1. Validation of numerical results

Fig. 8(a) and (b) shows the comparisons of the tangential velocity at the touching down stage, $S_E = 2.0$, and at multi-vortex stage, $S_E = 3.8$, respectively. The numerical data are from the stationary tornado over smooth ground. It is found that numerical results in this study show good agreement with experiment data, validating the numerical models applied in the present study.

3.2. Visualization of flow fields

In order to provide a general image on the tornado translation and ground roughness effects, the flow fields are visualized by instantaneous vorticity magnitude as shown from Figs. 9–11, vectors of time averaged flow fields as shown from Figs. 12–14, and time averaged tangential velocity contours as shown from Figs. 15–17.

From the instantaneous flow fields, it could be found that as the swirl ratio is increased, the stationary tornado-like vortex over smooth ground goes through various stages, see Fig. 11. For S_E=0.6, a vortex breakdown occurs. A very narrow core in the lower portion moves upward until it suddenly expands into a recirculation bubble, which is shown by a dashed square in Fig. 11 (a). In the transition region, the flow is typically turbulent. The animation of the vorticity shows that the breakdown is unstable and oscillates about a mean position. The radius of the vortex core increases and the altitude of the breakdown decreases as the swirl ratio increases. At S_E=2.0, see Fig. 11(b), the radial jet and the downward jet break away from the vertical axis at the low layer and generate a stretched bubble. A further increase in the swirl

ratio results in the breakdown being forced further toward the surface layer. The core of the vortex expands substantially and leaves a relatively calm inner sub-core, which is shown in Fig. 11 (c). For the translating tornado over smooth ground, see Fig. 12, it is clear that the introduction of tornado translation will disturb the flow fields near the ground and make the flow fields un-symmetry, whereas the major configurations do not show large change. At high elevation, the effects from tornado translation become not obvious. For the stationary tornado over rough ground, see Fig. 13, the introduction of ground roughness changes the configuration of tornado at S_E=0.6 greatly. Firstly, the vortex bubble dismisses. Secondly, the flow fields become laminar. Lastly, the core size decreases a lot. For S_E=2.0 and S_E=3.8, the flow fields seem not sensitive to the introduction of ground roughness. More detailed quantitative discussion about the effects from tornado translation and ground roughness will be presented in the following sections where the profiles of mean velocities and Reynolds stresses will be provided.

Figs. 13 and 16 show time averaged flow fields of tornado-like vortices with translation. Comparing the plots of stationary tornadoes over smooth ground, tornado translation breaks the symmetry of flow fields. At $S_E = 0.6$, the influence from translation is significant. When S_E is increased to 2.0 and 3.8, vortices incline is found to be concentrated in the region below 0.1 m. It can be found that, because of the added shear stress on the ground surface, on the side of vortex, where the motion of the ground surface is aligned with that of the fluid, the radial momentum is enhanced while on the opposite side it is reduced.

Figs. 14 and 17 show the time averaged flow fields of tornado-like vortices over rough ground. Solid lines indicate the height of roughness canopy. In Figs. 14(a) and 17(a), it is clearly shown that at $S_E = 0.6$, the introduction of roughness on the ground dismisses the expanded bubble, which makes flow fields much similar to those at the single-celled vortex stage. This means that at the vortex breakdown stage, the introduction of roughness provides similar effects in reducing the external swirl ratio, as mentioned by Natarajan and Hangan (2012). When S_E is increased to 2.0, see Fig. 14(b), the downward flow is stopped in the roughness canopy. Therefore, the force moving flow particles outward becomes weaker, as a result $r_{v\,max}$, which is the height of the location of V_{max}, is smaller than that over smooth ground, as illustrated in Table 8. At $S_E = 3.8$, flow fields are almost the same as those in the smooth case. An important characteristic is that the height at which the maximum tangential velocity appears is not affected by the roughness, which keeps as almost a constant of 0.01 m after Case5, as illustrated in Table 8.

3.3. Representative parameters

Same as the previous studies (see, Diamond and Wilkins (1984); Natarajan and Hangan (2012), Zhang and Sarkar (2008)), the inflow angle was kept as a constant for each case, so as to investigate how flow fields change with translation or roughness. The translating vortex over smooth ground and the stationary vortex over rough ground are examined and 9 cases are simulated for each group. The tornado vortex parameters are summarized in Table 8, where r_c is radius where V_c occurs, U_{min} is the minimum mean radial velocity, V_{max} is the universally maximum mean tangential velocity, W_{max} is the maximum mean vertical velocity, $r_{v\,max}$ and $h_{v\,max}$ are the radius and height of the location of V_{max} respectively, and P_{min} is the minimum pressure on the ground.

The disturbance of the axisymmetry of the tornado-like vortex due to translation brings difficulty to identify core radius, therefore it is meaningful to give a brief introduction of the way to determine these parameters. In the radar observation by Wurman and Alexander (2005), the data of the flow fields in a translating tornado were input into a purely axisymmetrical model. In this study, the same method is used and the space averaged value at each position is obtained by calculating mean of time averaged values over 12 azimuthal angles at the same radius and height. V_c, V_{max}, r_c, and $r_{v\,max}$ are then identified from this averaged flow field. All of the profiles plotted in this study are obtained from the averaged flow fields.

3.4. Similarity of tornado-like vortices

In order to show the effects of translation and roughness on similarity of tornado-like vortices, a number of representative non-dimensional parameters for the surface intensification are examined as shown in Table 9. The ratios V_{max}/V_c, $-U_{min}/V_{max}$, W_{max}/V_{max} and r_{vmax}/h_{vmax} are demonstrated as a function of the local corner swirl ratio, see Fig. 18. There is a shape peak near $S_c = 2.0$ for the ratio of V_{max} to V_c. Another important point is that after the introduction of the roughness, the intensification becomes stronger. For the cases of $S_c > 2.0$, V_{max}/V_c is almost constant around about 1.4. In Fig. 18(b), the ratio of $-U_{min}$ to V_{max} is presented. Having the same tendency, the results from the three situations scattered around a value of 0.65. In Fig. 18(c), peaks of W_{max}/V_{max} are found, which reach the highest value when the local corner swirl ratio is approximately 2.0. For the cases of $S_c > 2.0$, the ratio of W_{max}/V_{max} varies around an average value of 0.4. In Fig. 18(d), the geometry parameter ($r_{v\,max}/h_{v\,max}$) is illustrated and an appropriate linear relationship is shown with S_c. It is concluded that the surface intensification is determined by the local corner swirl ratio, S_c, and almost independent of translation speed and ground roughness.

It is important to find the length scale and the velocity scale of the numerical simulator. Hangan and Kim (2008), and Refan et al. (2014) proposed the length ratio $r_L = r_{v\,max}/h_{v\,max}$ to match the simulated vortices to the full scale Spencer tornado with $r_L = 6.0$ obtained from the data provided by Kuai et al. (2008). Matching the simulated vortex ($r_L = 6.3$) at $S_E = 3.8$ of the stationary tornado over smooth ground with the Spencer tornado, it is found that the length scale, $r_{v\,max,m}/r_{v\,max,p}$, is 1:1905 and the velocity scale, $V_{max,m}/V_{max,p}$, is 1:3.05, in which $r_{max,p}$ is 120 m and $V_{max,p}$ is 81 m/s. Subscripts "m" and "p" respectively represent the values in numerical simulations and Spencer tornado. Furthermore, scaled V_c and r_c in Case9 are compared with those in the Spencer tornado, which are 57 m/s and 213 m in Case9 and 65 m/s and 220 m in the Spencer tornado. The detailed discussion concerning the method to scale tornado in simulation can be found in the study conducted by Liu and Ishihara (2015a).

As mentioned above, the case that external swirl ratio $S_E = 3.8$ corresponds to Spencer tornado occurred in the countryside. The smooth ground is taken into consideration and the scaled translation speed of 10 m/s is added in Case9, which is equal to 3.3 m/s in the simulation. As shown in Fig. 19, normalized tangential velocity and radial velocity are respectively plotted in radial and vertical directions and the observation data in the Spencer tornado are adapted from the study of Haan et al. (2008) in which the profiles are normalized by r_c and V_c. The comparison with stationary cases demonstrates that simulated tangential velocities are improved near the ground and radial velocities become much closer to those of Spencer tornado after the introduction of translation. Eventually, it is concluded that the tornado in nature can be well reproduced in consideration of tornado translation speed.

In Fig. 20, comparison of normalized tangential velocity and radial velocity over smooth and rough ground is also demonstrated with the external swirl ratio of $S_E = 3.8$. Tangential velocities near the ground are found to be comparable. At the height of $z = 0.52r_c$, there are some discrepancies near the center. However, the peak location and the magnitude show good agreement. At

high elevations, radial velocities show some differences. Nevertheless, differences between them become small near the ground. Furthermore, these two tornadoes have almost the same local corner swirl ratios, which indicates that S_c is a determinant factor for the surface intensification.

4. Turbulent flow fields of translating tornado

From this section, the flow fields will be normalized by r_0 in space and W_0 for velocities to show the effects from tornado translation or the ground roughness, because r_0 and W_0 do not change with the swirl ratio and the condition of the bottom of tornado simulator.

The introduction of tornado translation disturbs the space averaged flow of tornado-like vortices slightly as shown in Fig. 21, where the maximum tangential velocity in the cyclostrophic balance region V_c and the core radius r_c with S_E are plotted. Overall it can be concluded that V_c and r_c are not sensitive to tornado translation.

4.1. Mean flow fields of translating tornado

For the radial velocity, the profile shape at $S_E = 0.6$ does not change too much, as shown in Fig. 22(a). In the cyclostrophic balance region, the magnitude of the radial velocity is almost zero for translating and stationary tornadoes, which means that at high level, flow fields still follow the cyclostrophic balance law. When S_E is increased to 2.0, tornado translation makes the inversion point closer to the center, while no large difference is observed in the outer region. As shown in Fig. 22(c), the radial velocity shows similar distributions with the stationary case at the large swirl ratio, $S_E = 3.8$.

In Fig. 23, radial distribution of the space averaged tangential velocity is presented for translating and stationary cases. When the external swirl ratio equals to 0.6, the tangential velocity decreases slightly with the introduction of translation, as shown in Fig. 23(a). When S_E is increased to 2.0, the tangential velocity profile changes in the outer region, $r > r_c$. As shown in Fig. 23(b), non-zero values in the center are less than those at $S_E = 0.6$. This means that the tornado incline becomes weak. For the case of large swirl at $S_E = 3.8$, the profile of tangential velocity of translating tornado is almost identical with that of stationary tornado in the cyclostrophic balance region, which implies that the tornado becomes less sensitive to motion. Near the ground, the peak of tangential velocity moves towards inner after adding translation.

It is clear that after the introduction of the translation, the vertical velocity at $S_E = 0.6$ changes a lot, as shown in Fig. 24(a). At low elevation, the peak value decreases from $2.8W_0$ to $0.5W_0$. On the other hand, at the height of $1.0r_0$, the sharp decrease is smoothed due to the disturbance from translation even though the peak values are almost the same. In the outer range of the tornado, the vertical velocity profile becomes the same as that of stationary tornado. As shown in Fig. 24(b) and (c), the effect of translation on the vertical velocity becomes weak when $S_E = 2.0$ and 3.8.

In addition, the translation brings a number of changes to the profile of ground pressure normalized by $1/2\rho W_0^2$, as shown in Fig. 25. For these three cases, pressure drops become less than those of stationary tornados, since tangential velocities decrease near the ground when translation is introduced.

In order to give an explanation of translating effects to the size of tornado, the ratio of tangential momentum to radial momentum at $z = h_{v\ max}$ is shown in Fig. 26. This parameter shows how the swirl is enhanced or weakened near the ground. Since the flow fields in the core is very complicated, momentum ratio in the outer region, $r > r_c$, are investigated. The momentum ratio is found to be not sensitive to translation. This should be the answer why the size of tornado does not change much after the introduction of tornado translation.

4.2. Reynolds stresses of translating tornado

Through a detailed examination of the turbulent flow fields for tornado-like vortices at touch-down, Ishihara and Liu (2014) indicated that it is not sufficient to characterize only the mean flow fields because the turbulent characteristics are also important for tornado-like vortices. Recently, Liu and Ishihara (2015a) provided detailed turbulent information for the tornado-like vortices with different swirl ratios by large eddy simulations; however, the study about the turbulent information of the tornadoes with translation and those over roughness is limited. Therefore, the turbulent aspects of the tornado-like vortices with translation and those over roughness are also studied systematically. Herein, the turbulent characteristics are quantitatively examined using Reynolds normal stresses, i.e. u', v' and w', and shear stresses, i.e., $u'v'$, $u'w'$, and $v'w'$.

Figs. 27–29 present the horizontal profiles of root mean square of the radial, tangential and vertical fluctuations, from which it can be found that the fluctuations of the tornadoes with translation show similar trend with the stationary ones. When the swirl ratio is 0.6 the Reynolds normal stresses at both low elevation $z=h_{vmax}$ and high elevation $z=r_0$ show peaks at the center of the tornado no matter the tornado is translating or no. But, the peak values of v' and w' of the tornado with translation are less than those of stationary tornado. This is because that the gradients of mean tangential velocity and mean radial velocity become less after the introduction of translation. Compared with u' and v', the vertical fluctuation w' are quite large which results from the unsteadiness of the breakdown bubble along the vertical axis as has been pointed out in the study by Liu and Ishihara (2015a). When the swirl ration is 2.0 or 3.8, at the low elevation $z=h_{vmax}$, the Reynolds normal stresses of the translating tornado are globally larger than those of the stationary ones. The increase of the Reynolds normal stresses near the ground is due to the disturbance of the flow from the introduction of tornado translation. However, the increase is not large and the locations of the peaks in the horizontal profiles are almost same. Different with the stages of $S_E=0.6$, the peaks of the Reynolds normal stresses are not at the center of tornado but near the outer ring of the core, which is due to the factor that after the vortex touch down stage ($S_E \geq 1.0$) the central downward flow touches the ground and interacts with the inward radial flow. At the high elevation, for the cases of $S_E=2.0$ and $S_E=3.8$ the increase of Reynolds normal stresses becomes weak.

Figs. 30–32 present the horizontal profiles of the Reynolds shear stresses. Overall the Reynolds shear stresses of the tornado with translation are comparable with those without translation. The locations and the magnitudes of peaks nearly coincide. The shear stress is less than the normal stresses with one order of magnitude. Different with the stages of $S_E=2.0$ and $S_E=3.8$, at the stage of $S_E=0.6$ the Reynolds shear stresses $u'w'$ and $v'w'$ show much larger values at $z=1.0r_0$ than those at $z=h_{vmax}$, this is because that the breakdown bubble could not reach to the very low locations.

5. Turbulent flow fields of tornado over ground roughness

As shown in Fig. 33(a), the introduction of ground roughness brings some changes to V_c. When the external swirl ratio is small, V_c increases with the increase of ground roughness. Nevertheless, this effect is reversed when the external swirl ratio is large. In addition, the effect of roughness on V_c is small, which indicates

that V_c is dominated by the inflow angle. As shown in Fig. 33(b), the core radius, r_c, changes obviously when the ground is rough. For the cases of low external swirl ratio, the ground roughness reduces the core size. For the external swirl ratio between 0.8 and 3.3, the ground roughness expands the tornado core size and exhibits the largest expansion at $S_E = 1.5$.

5.1. Mean flow fields of tornado over roughness

As shown in Fig. 34(a), the roughness show slight effects at $S_E = 0.6$ for the radial velocity. But for the case of $S_E = 2.0$, radial velocity profiles changes a lot. In addition, the inward radial flow penetrates to the center and the stagnation ring in the smooth ground case becomes almost one stagnation point located at the center. This development from stagnation ring to stagnation point indicates that the inner downward flow does not touch the ground. At the multi-vortex stage of $S_E = 3.8$, after adding the roughness, the stagnation ring becomes smaller. However, when $r > r_0$, the radial velocity becomes almost the same as that of the smooth cases.

In Fig. 35(a), profiles of tangential velocities at $S_E = 0.6$ are shown. It is clear that after the introduction of the roughness, the overshoot near ground disappears. Besides, the peak of the tangential velocity at $z = h_{v\ max}$ becomes smaller than that at $z = 1.0r_0$, which indicates that the flow pattern changes to single-celled vortex agreeing with the above discussions of visualized flow fields. At $S_E = 2.0$, the obvious change is the profile at $z = 1.0r_0$, as shown in Fig. 35(b), where the peak is pushed outward. In the outer region, the effects from roughness becomes weak and the profile at $z = 1.0r_0$ agrees well with that over smooth ground. For $S_E = 3.8$, the peak tangential velocity at $z = h_{v\ max}$ is smaller than that of tornado over smooth ground and the location of this peak tangential velocity becomes closer to the center. In the cyclostrophic balance region, tangential profiles of these two cases are almost consistent.

Fig. 36 shows the radial distribution of the vertical velocity. For the case of $S_E = 0.6$, the same profile can be found in the outer region. Nevertheless, due to the introduction of the roughness, profiles at high and low elevations changes significantly in the inner part. Large vertical velocity is found in the center and when the ground is rough, the magnitude increases with height. As mentioned by Ishihara et al. (2011), this is the typical distribution of the vertical velocity for single-celled vortex. As shown in Fig. 36 (b), the roughness makes the central flow difficult to touch the ground and the vertical velocity shows the positive value at $S_E = 2.0$. When $S_E = 3.8$, the profile at the cyclostrophic balance region is flattened and the region with negative value becomes narrow.

In addition, the introduction of roughness has an effect on the pressure distribution on the ground. As shown in Fig. 37, the pressure drop becomes weak. At $S_E = 3.8$, due to the weakened touching down of the flow, the pressure profile near the center is sharper when compared with that in smooth case.

In order to give some explanations of roughness effects, the ratio of tangential momentum to radial momentum is shown in Fig. 38. On account of the mass conservation, the ground roughness is difficult to decrease the radial wind speed, while the tangential velocity is decreased by the roughness drag. When compared with the tornado over smooth ground, the absolute value of momentum ratio decreases a lot near the center. It means that the swirling strength decreases and the flow pattern changes from vortex breakdown to single-celled vortex. This is the reason why the core radius is reduced by half. As will be discussed below the vortex bubble touches on the roughness and the interaction between the roughness and the vortex bubble generates much more turbulence for the case of $S_E = 2.0$. Even though the momentum ratio is reduced in this case, this increased turbulence expands the tornado core. At the multi-vortex stage with $S_E = 3.8$, the roughness decreases the momentum ratio, while the turbulence is generally increased. The momentum ratio reduction has the effect of reducing the core radius, however the turbulence increase can expand the tornado core. From Fig. 33(b), it is found that the core size does not change so much at $S_E = 3.8$ and this is possibly due to the canceling out of the above two effects.

5.2. Reynolds stresses of tornado over roughness

Horizontal profiles of the Reynolds normal stresses are shown from Figs. 39–41. When $S_E = 0.6$, it can be found three components of the turbulence fluctuations are overall decreased by the introduction of ground roughness, especially for the vertical component whose peak value becomes only one third of that with smooth ground, showing similar features with the stage of single-celled vortex. For $S_E = 2.0$, the peaks of mean tangential, radial and vertical velocities at height of h_{vmax} move close to the center of tornado when the ground is rough as shown in the above subsection, as a result it can be imagine that the fluctuations of the tangential, radial and vertical components at $z = h_{vmax}$ will be also closer to the center as could be found from Figs. 39–41. At the high elevation, $z = 1.0r_0$, the influence from the ground roughness becomes weak for the radial and vertical components. But for the tangential component, the introduction of ground roughness will increase the value, which is believed to be the reason of the expansion of the tornado at this stage. When $S_E = 3.8$, the turbulence fluctuations becomes much smaller at the low elevation after the introduction of roughness. The peaks of the profiles move to the center of tornado. At high elevation, all of the components show similar results between the cases with ground roughness and those without. The tangential component gives some increase in the region from $r = 0.5r_0$ to $r = 1.0_{r0}$ after the introduction of roughness and another peak locates at $r = 0.75r_0$ appears.

Reynolds shear stresses are shown from Figs. 42–44. For $S_E = 0.6$, it can be found the introduction of ground roughness makes the Reynolds shear stresses become smaller than those over smooth ground with one order of magnitude. This is due to the factor that the configuration of tornado has been changed from vortex breakdown to single-celled vortex. For $S_E = 2.0$, we can see that the influence from the ground roughness increases the Reynolds shear stresses at both low and high elevations. For $S_E = 3.8$, the Reynolds shear stresses at high elevation do not show large difference after the introduction of roughness. But at low elevation, the Reynolds shear stresses are restrained.

6. Conclusions

In this study, the effects of translation and roughness on turbulent flow fields of tornado-like vortices are examined and conclusions are summarized as follows:

(1) The translation disturbs tornado symmetry and at the center of tornado, the space averaged tangential velocity becomes non-zero. The shear stress added on the surface increases the turbulence at low elevation and at the stage of vortex breakdown, overshoots for tangential velocity and vertical velocity are smoothed. In nature, the tornado is also well reproduced in consideration of the tornado translation speed.
(2) At the vortex breakdown stage, tornado configuration changes to single-celled vortex after the introduction of roughness, which results in tornado shrink. At the stage of vortex touching down, the turbulence is increased by the interaction between the touching down bubble and the roughness and

the tornado core is enlarged. After the vortex touching down stage, the height and value of the maximum tangential velocity is not strongly affected by the ground roughness.

(3) For the cases that S_c is larger than 2.0, the following parameters show the same tendency, such as V_{max}/V_c, $-U_{min}/V_{max}$, W_{max}/V_{max} and $r_{v\,max}/h_{v\,max}$, which means that for large swirl situations, the local corner swirl ratio is applicable to determine the flow fields near the ground.

References

Church, C.R., Snow, J.T., Baker, G.L., Agee, E.M., 1979. Characteristics of tornado-like vortices as a function of swirl ratio: a laboratory investigation. J. Atmos. Sci. 36, 1755–1776.

Dessens, J.J., 1972. Influence of ground roughness on tornadoes: a laboratory simulation. J. Appl. Meteorol. 11, 72–75.

Diamond, C.J., Wilkins, E.M., 1984. Translation effects on simulated tornadoes. J. Atmos. Sci. 41, 2574–2580.

Doswell III, C.A., Carbin, G.W., Brooks, H.E., 2012. The tornadoes of spring 2011 in the USA: an historical perspective. Weather 67, 88–94.

Ferziger, J., Peric, M., 2002. Computational Method for Fluid Dynamics, 3rd ed. Springer, Berlin.

Haan, F.L., Sarkar, P.P., Gallus, W.A., 2008. Design, construction and performance of a large tornado simulator for wind engineering applications. Eng. Struct. 30, 1146–1159.

Hangan, H., Kim, J.-D., 2008. Swirl ratio effects on tornado vortices in relation to the Fujita scale. Wind Struct. 11, 291–302.

Ishihara, T., Oh, S., Tokuyama, Y., 2011. Numerical study on flow fields of tornado-like vortices using the LES turbulence model. J. Wind Eng. Ind. Aerodyn. 99, 239–248.

Ishihara, T., Liu, Z., 2014. Numerical study on dynamics of a tornado-like vortex with touching down by using the LES turbulent model. Wind Struct. 19, 89–111.

Kim, J., Hangan, H., 2007. Numerical simulations of impinging jets with application to downbursts. J. Wind Eng. Ind. Aerodyn. 2007 (95), 279–298.

Kuai, L., Haan, F.L., Gallus, W.A., Sarkar, P.P., 2008. CFD simulations of the flow field of a laboratory-simulated tornado for parameter sensitivity studies and comparison with field measurements. Wind Struct. 11, 1–22.

Leslie, F.W., 1977. Surface roughness effects on suction vortex formation: a laboratory simulation. J. Atmos. Sci. 34, 1022–1027.

Lewellen, D.C., Lewellen, W.S., Xia, J., 2000. The influence of a local swirl ratio on tornado intensification near the surface. J. Atmos. Sci. 57, 527–544.

Liu, Z., Ishihara, T., 2015a. Numerical study of turbulent flow fields and the similarity of tornado vortices using large-eddy simulations. J. Wind Eng. Ind. Aerodyn. 145, 42–60.

Liu, Z., Ishihara, T., 2015b. A study of tornado induced mean aerodynamic forces on a gable-roofed building by the large eddy simulations. J. Wind Eng. Ind. Aerodyn. 146, 39–50.

Maruyama, T., 1993. Optimization of roughness parameters for staggered arrayed cubic blocks using experimental data. J. Wind Eng. Ind. Aerodyn. 46–47, 165–171.

Maruyama, T., 2011. Simulation of flying debris using a numerically generated tornado-like vortex. J. Wind Eng. Ind. Aerodyn. 99, 249–256.

Matsui, M., Tamura, Y., 2009, Influence of swirl ratio and incident flow conditions on generation of tornado-like vortex. In: Proc. of EACWE. 5, CD-ROM.

Mishra, A.R., James, D.L., Lethcford, C.W., 2008. Physical simulation of a single-celled tornado-like vortex, Part A: flow field characterization. J. Wind Eng. Ind. Aerodyn. 96, 1243–1257.

Monji, N., 1985. A laboratory investigation of the structure of multiple vortices. J. Meteorol. Soc. Jpn. 63, 703–712.

Monji, N., Wang, Y., 1989. A laboratory investigation of characteristics of tornado-like vortices over various rough surfaces. ACTA Meteorol. Sin. 47, 34–42 (In Chinese).

Natarajan, D., Hangan, H., 2012. Large eddy simulation of translation and surface roughness effects on torando-like vortices. J. Wind Eng. Ind. Aerodyn. 104–106, 577–584.

Refan, M., Hangan, H., Wurman, J., 2014. Reproducing tornadoes in laboratory using proper scaling. J. Wind Eng. Ind. Aerodyn. 135, 136–148.

Rotunno, R., 1977. Numerical simulation of a laboratory vortex. J. Atmos. Sci. 34, 1942–1956.

Tari, P.H., Gurka, R., Hangan, H., 2010. Experimental investigation of tornado-like vortex dynamics with swirl ratio: the mean and turbulent flow fields. J. Wind Eng. Ind. Aerodyn. 98, 936–944.

Ward, N.B., 1972. The exploration of certain features of tornado dynamics using a laboratory model. J. Atmos. Sci. 29, 1194–1204.

Wilson, T., Rotunno, R., 1986. Numerical simulation of a laminar end-wall vortex and boundary layer. Phys. Fluids 29, 3993–4005.

Wurman, J., Alexander, C.R., 2005. The 30 may 1998 spencer, south dakota, storm. Part II: comparison of observed damage and radar-derived winds in the tornadoes. Mon. Weather Rev. 133, 97–119.

Zhang, W., Sarkar P., 2008, Effects of ground roughness on tornado-like vortex using PIV, AAWE Workshop, Aug 21–22, Vail, Colorado.